Dramatic changes in atmospheric pollution source contributions for a coastal megacity in northern China from 2011 to 2020

Baoshuang Liu[1,2], Yanyang Wang[1,2], He Meng[3], Qili Dai[1,2], Liuli Diao[1,2], Jianhui Wu[1,2], Laiyuan Shi[3], Jing Wang[3], Yufen Zhang[1,2*], and Yinchang Feng[1,2*]

[1]State Environmental Protection Key Laboratory of Urban Ambient Air Particulate Matter Pollution Prevention and Control & Tianjin Key Laboratory of Urban Transport Emission Research, College of Environmental Science and Engineering, Nankai University, Tianjin, 300350, China

[2]CMA-NKU Cooperative Laboratory for Atmospheric Environment-Health Research, Tianjin 300350, China

[3]Qingdao Eco-environment Monitoring Center of Shandong Province, Qingdao, 266003, China

Correspondence to: Y.F. Zhang (zhafox@nankai.edu.cn) and Y.C. Feng (fengyc@nankai.edu.cn)

Abstract

Understanding the effectiveness of long-term air pollution regulatory measures is important for control policy formulation. Efforts have been made using chemical transport modelling and statistical approaches to evaluate the efficacy of the Clean Air Action Plan (2013-2017, CAAP) and the Blue Sky Protection Campaign (2018-2020, BSPC) enacted in China. Changes in air quality due to reduction in emissions can be masked by meteorology, making it highly challenging to reveal the real effects of control measures. Knowledge gap still existed with respect to how sources changed before and after the CAAP and BSPC implemented, respectively, particularly in coastal area where anthropogenic emissions mixed with additional natural sources (e.g., marine aerosol). This work applied a machine learning-based meteorological normalization approach to decouple the meteorological effects from air quality trend in a coastal city in northern China (Qingdao). Secondly, the relative changes in source contributions to ambient $PM_{2.5}$ with a ~10-year observation interval (2011-2012, 2016, and 2019) were also investigated. We discovered that the largest emission reduction section was likely from coal combustions, as the meteorologically normalized SO_2 dropped by ~15.5% yr^{-1} and dispersion normalized SO_4^{2-} decreased by ~41.5% for annual average. Change in the meteorologically normalized NO_2 was relatively stable (~1.0% yr^{-1}), and NO_3^- changed inappreciable in 2016-2019 but significantly higher than that prior to the CAAP. Crustal dust decreased remarkably after the CAAP began. Industrial emissions, for example, steel-related smelting, decreased after 2016 due to the relocation of steelmaking enterprises. Note that vehicle emissions were increased in importance, as opposed to the other primary sources. Similar to other mega cities, Qingdao also risks increased ozone pollution that in turns facilitate secondary particles formation in the future. The policy assessment approaches applied in this work also work for other places where air quality management is highly in demand to reduce air pollution.

Key words: Air quality; Random forest; Dispersion normalization; Source apportionment; Coastal megacity

1 Introduction

Rapid industrial development and energy consumption in China over the past several decades have resulted in severe air pollution (Dai et al., 2021; Huang et al., 2014; Zhang et al., 2012). Fine particulate matter ($PM_{2.5}$, particles with aerodynamic diameter $\leq$ 2.5 μm) is the leading health-risk factor for attributable mortality in China (Cohen et al., 2017). It is well-documented that exposure to $PM_{2.5}$ has been associated with increased mortality (Joshi et al., 2021; Liu et al., 2021b; Vodonos and Schwartz, 2021). The World Health Organization recently set the annual average concentration of $PM_{2.5}$ to 5 μg m^{-3}. Most countries or regions are facing a great challenge now to meet the guideline since their current $PM_{2.5}$ levels are well above the latest threshold.

To alleviate the severe impact of air pollution on the living environment and public health, the State Council of China released a five-year "Air Pollution Prevention and Control Action Plan" in 2013 (hereinafter the "Clear Air Action Plan, CAAP") (http://www.gov.cn/zwgk/2013-09/12/content_2486773.htm, last access: 29 October 2021). This was followed by the tighter "Three-year Action Plan to the Blue Sky Protection Campaign" (hereinafter the "Blue Sky Protection Campaign, BSPC") in 2018 (http://www.gov.cn/zhengce/content/2018-07/03/content_5303158.htm, last access: 29 October 2021). The executions of these measures significantly improved air quality (Jiang et al., 2021), thus gained appreciable health benefits (Huang et al., 2018). Vu et al. (2019) demonstrated that the control measures requested by the CAAP have tremendously reduced the emissions in $PM_{2.5}$, PM_{10}, NO_2, SO_2, and CO in Beijing from 2013 to 2017 by approximately 34%, 24%, 17%, 68%, and 33%, respectively. Xu et al. (2021) found that by 2020, $PM_{2.5}$ reduction measures avoided 3561 thousand morbidity cases and 24 thousand premature deaths in the Beijing-Tianjin-Hebei region.

Evaluation of the effectiveness of air pollution controls is important for control policy formulation to further improve future air quality (Dai et al., 2020). Many studies have been carried out to evaluate the efficacy of control measures around the world. For example, assessments on short-term control measures were made for the 2008 Olympic Games (Schleicher et al., 2012), 2013 Second Asian Youth Games in Nanjing (Qi et al., 2016), 2014 Asia Pacific Economic Cooperation (Xu et al., 2019b), 2015 Military Parade (Wang et al.,

80   2017), and 2017 Belt and Road Forum for International Cooperation (Ma et al., 2020), as

81   well as the 2020 COVID-19 worldwide lockdown (Beloconi et al., 2021; Chen et al., 2020b;

82   Cucciniello et al., 2022; Shi et al., 2021; Wang et al., 2021a). Medium-term (3–5 years)

83   evaluations on the validity of control measures have also been examined (Li et al., 2021b; Yu

84   et al., 2019; Zhang et al., 2019). In contrast, long-term (~10 years) evaluations on controls

85   were rarely reported (Masiol et al., 2019). The majority of such studies have focused

86   primarily on the changes in concentrations of criterion air pollutants to qualitatively deduce

87   the efficacy of source control (Cheng et al., 2019; Lyu et al., 2017; Li et al., 2020b; Wang et

88   al., 2014). For example, Vu et al. (2019) and Liang et al. (2016) applied random forest and

89   non-parametric methods to normalize the impact of meteorological factors to evaluate the

90   changes in air pollutant concentrations and the effect of control measures in Beijing and other

91   cities in China over recent time periods. However, quantitative evaluations of source

92   emissions have not been common (Gulia et al., 2018), due to the lack of long-term particle

93   composition monitoring (Hopke et al., 2020) and only a handful of studies quantitatively

94   assessing source contributions smoothed the disturbance of weather conditions.

95   Qingdao, as an economically developed coastal megacity in northern China, has suffered

96   severe air pollution (Bie et al., 2021; Gao et al., 2020; Li et al., 2017). It has been reported

97   by Li et al. (2021a) that meteorology plays a critical role in the formation of pollution for this

98   coastal region. In addition, based on measures taken in accordance with the "CAAP" since

99   2013 and the "BSPC" since 2018, source interventions such as the relocation and

100 transformation of businesses and industries from the Old Town to port regions (Liu et al.,

101 2021a) have been implemented to improve the air quality in Qingdao. Up to now, the air

102 quality in Qingdao has been greatly improved. Liu et al. (2020a) assessed the changes in O_3

103 concentrations during the Shanghai Cooperation Organization (SCO) Summit in Qingdao and

104 analyzed the impact of control measures on the emissions reduction of its precursors, and Liu

105 et al. (2020b) also analyzed the reasons for the increase of O_3 concentration at nighttime

106 during the SCO Summit. However, there is no report to date has evaluated the effectiveness

107 of these control measures based on a long-term time scale after these control measures were

108 put into practice, especially for quantitating the changes in source contributions by smoothing

109 the influences of weather conditions. In view of this, our work was mainly to evaluate the

110 implementation of control measures utilizing the data of weather-normalized air pollutants,

111 changes in chemical compositions in $PM_{2.5}$ and source contributions as well as extra source

112 origins from 2011 to 2020. Findings of this work are expected to provide the basis for policy

113 development for a coastal megacity in the future.

114

115 **2 Materials and methods**

116 2.1 Study region and sampling site

117 Qingdao is an economically developed coastal megacity of Shandong province, China

118 (Fig. S1). The variation of local economic and social developments from 2011 to 2019 were

119 counted and are shown in Fig. S2. During this period, the local resident population continued

120 to rise, reaching 9499.8 thousand in 2019. The developed area and the possession of civil

121 motor vehicles also showed upward tendency, attaining 758.2 km^2 and 3062 thousand units in

122 2019, respectively. The total energy consumption had a maximum of 16891 thousand tons

123 standard coal in 2012 and maintained comparable levels from 2014 to 2019. The industrial

124 coal burning capacity above the designated scale and the volume of liquefied petroleum

125 supply both presented downward trend with values of 10965.7 and 30.2 thousand tons in

126 2019, respectively. The emissions of sulfur dioxide, nitrogen oxide, and dust basically

127 showed a downward trend from 2011 to 2019, especially in 2017, and the emissions of these

128 pollutants remained at relatively low levels after 2017, reflecting that the pollution sources

129 for these particular pollutants had been effectively controlled in Qingdao.

130 In this study, in order to evaluate the effectiveness of control measures targeted for

131 polluted sources in the past decade in Qingdao, ambient $PM_{2.5}$ samples were collected at

132 urban sites over three time periods during 2011-2012, 2016, and 2019. The 2011-2012

133 samples were collected before the "CAAP" was enacted in 2013, and the 2016 samples were

134 collected at the end of the "CAAP", while the 2019 samples were collected during the

135 middle of the "BSPC" policy period. The sampling plan (detailed in the next section) was

136 designed to capture changes in the data during these periods, as any changes could reflect

137 changes in the pollution sources during different stages of China's air pollution control

138 measures. The sites of Licang and Shinan were sampled in 2011-2012, while five additional

139 sites, Shibei, Laoshan, Chengyang, Huangdao, and Jiaonan were sampled in 2016 and 2019

140   (Fig. S1). All collection sites were situated on building rooftops ~10–15 m above ground

141   level and used to collect ambient $PM_{2.5}$ samples. Further descriptions of the seven sampling

142   sites are shown in Table S1.

143   2.2 Sampling and analysis

144   The sampling periods covered all seasons per year and lasted 41, 56, and 60 days for

145   2011-2012, 2016, and 2019, respectively (Table S2). Particles were gathered simultaneously

146   to polypropylene filters and quartz filters loaded to sampling instruments. The details of the

147   sampling instruments and filters in the different years are listed in Table S3. Samples were

148   collected for a duration of 22 h from 11:00 to 09:00 of the next day. Field blanks and parallel

149   samples were synchronously collected at each site. Before sampling, to remove some volatile

150   compounds and impurities, the quartz and polypropylene filters were baked in an oven at 500

151   °C and 60 °C for 2 h, respectively. After sampling, all the filters were stored at 4 °C before

152   gravimetric and chemical analyses were conducted.

153   Before gravimetric analysis, filter equilibration for 48 h was needed under a constant

154   temperature (20 ± 1 °C) and humidity (45–55%). All filters were weighed by the

155   microbalances with a resolution of 1 or 10 μg during different sampling periods; detailed

156   information is listed in Table S4. To ensure the accuracy, static was eliminated before

157   weighting and all filters were weighed at least twice to meet error requirements (Table S4).

158   For chemical analysis, the elements of Na, Mg, Al, Si, K, Ca, Ti, V, Mn, Fe, Ni, Cu, Zn, and

159   Pb were analyzed in different years. For samples collected in 2011-2012 and 2016,

160   inductively coupled plasma-mass spectrometer (ICP-MS) was applied to determine these

161   elements. For samples collected in 2019, inductively coupled plasma-optical emission

162   spectrometer (ICP-OES) was used to measure all related elements. Water-soluble inorganic

163   ions of NO_3^-, SO_4^{2-}, NH_4^+, and Cl^- were determined using the ion chromatographs during

164   different years. The organic carbon (OC) and elemental carbon (EC) of samples during

165   different years were determined using a thermal/optical carbon analyzer, based on the

166   IMPROVE (in 2011-2012) and IMPROVE_A (in 2016 and 2019) thermal/optical reflectance

167   protocol. The detailed instrumental information is listed in Table S5 and analysis procedures

168   and quality controls are described in Text S1 in the supplemental materials as well as prior

169   works from Liu et al., 2021a), Huang et al. (2021), Wang et al. (2021b), and Tian et al.,

170   (2014).

171   2.3 Random forest (RF) based weather normalization

172   From 1 January 2015 to 31 December 2020, the hourly concentrations of six air

173   pollutants ($PM_{2.5}$, PM_{10}, SO_2, NO_2, CO, and O_3) at the nine national air quality monitoring

174   stations in Qingdao were collected from the China National Environmental Monitoring

175   Network (CNEM) (http://106.37.208.233:20035, last access: 29 October 2021). Data

176   collected from the nine monitoring stations were averaged to represent the pollution level at

177   city scale. The explanatory variables including the meteorological variables and time

178   variables were used to build the RF model and predict the air pollutant concentrations

179   Hourly surface meteorological data including wind speed, wind direction, temperature,

180   dewpoint, relative humidity, and pressure recorded at Qingdao Liuting International Airport

181   were downloaded using the "worldMet" R package (Carslaw, 2017). Time variables

182   included Unix time (number of seconds since 1 January 1970), Gregorian day (day of the

183   year), month, week, weekday, and hour of the day. Data were analyzed in RStudio with a

184   series of packages, and the details of the random forest (RF) model and weather

185   normalization using the RF model are provided in Vu et al. (2019). The training data set was

186   comprised of 80% of the whole data, with the rest as testing data. After the RF predictive

187   model was built for every pollutant, the model was then fed with a new dataset comprised of

188   time variables same with the original dataset and meteorological variables that resampled

189   from the whole observation. The prediction process was repeated 500 times to predict the

190   concentration of a pollutant. The 500 predicted concentrations were then averaged to

191   calculate the weather normalized concentration. The RF based weather normalization

192   technique has been extensively used to decouple meteorology from the observed

193   concentrations, thus can detect interventions in emissions over time (Dai et al., 2020;

194   Grange et al., 2018, 2019).

195

196   2.4 Theil-Sen regression

197   The Theil-Sen regression technique has been commonly used to explore the long-term

198   trend of pollutants over years. This approach assumes monotonic linear trends (Masiol et al.,

199   2019). Its principle is to calculate the slopes of all possible pairs of pollutant concentrations,

200   select the median value, and give accurate confidence intervals (Munir et al., 2013; Sen,

201   1968). In this study, the data of air pollutants obtained from RF modelling with weather

202   normalization was de-seasonalized as the Theil-Sen regression being performed. The Theil-

203   Sen function is provided by the "openair" R package.

204   2.5 Dispersion normalization

205   The concentrations of ambient particles are affected by both local emissions and

206   meteorological dispersion (Sujatha et al., 2016). Dispersion normalization helps stabilize the

207   variation of concentrations due to atmospheric dispersion (Sofowote et al., 2021); therefore,

208   in this study, the contributions of local emissions to particle concentrations were highlighted.

209   Research suggests that the quantities for particles dispersion can be determined by the

210   ventilation coefficient (VC) (Kleinman et al., 1976; Iyer and Raj, 2013), which is defined as

211   the multiplication of mixed layer height (MLH) and the mean wind speed (WS) within the

212   mixed layer (Eq. (1)). Basing on a VC at a given time interval i, the normalized concentration

213   can be obtained by Eq. (2):

$$VC_i = MLH_i \times WS_i \qquad (1)$$

$$C_{vc,i} = C_i \times \frac{VC_i}{VC_{mean}} \qquad (2)$$

216   where VC_i (m^2 s^{-1}) is the ventilation coefficient during period i, VC_{mean} (m^2 s^{-1}) is the mean

217   VC during the whole study period, and $C_{vc,i}$ (μg m^{-3}) and C_i (μg m^{-3}) are the normalized and

218   observed concentrations, respectively. In this study, the dispersion normalization was

219   conducted for ambient PM$_{2.5}$ and chemical compositions and the resolved source

220   contributions. The surface wind speed at 10 m was replaced with the mean wind speed

221   through MLH because of the absence of wind speed at different heights (Dai et al., 2020;

222   Ding et al., 2021). The 3 h resolution data of MLH and WS was derived from archived

223   meteorology of the National Ocean and Atmospheric Administration

224   (https://www.ready.noaa.gov/READYamet.php, last access: 29 October 2021), and the

225   calculated daily MLH and WS data were used in this study.

226   2.6 Positive matrix factorization (PMF)

227   In order to assess the effectiveness of pollution control, source categories and their

228   contribution were estimated by the PMF method. The PMF decomposes a sample

229 composition dataset (X) into two matrices including source profiles (F) and source

230 contributions (G) (Paatero and Tapper, 1994). This principle can be refined as follows:

231 $$x_{ij} = \sum_{k=1}^{p} g_{ik} f_{kj} + e_{ij} \qquad (3)$$

232 where x_{ij} is the concentration (μg m^{-3}) of the jth component from the ith sample; g_{ik} means the

233 contribution (μg m^{-3}) of the kth source to the ith sample; f_{kj} represents the source profile (μg

234 μg^{-1}) of the jth component from the kth source; e_{ij} is the residual (μg m^{-3}) of the jth

235 component of the ith sample; and p means the number of sources. In this study, US EPA PMF

236 v5.0 was applied to carry out source apportionment, and the details in treatment of input data

237 and method detection limits of chemical compositions are described in Table S6 and Text S2,

238 respectively. Bootstrap (BS) and displacement (DISP) analyses were used to investigate the

239 effects of measurement error and rotation ambiguity on the resulting solutions.

240 2.7 Potential source contribution function (PSCF)

241 We performed PSCF to further investigate the origin of polluted sources. First, the 72 h

242 backward trajectories were calculated at 6 h intervals every day with starting height of 100m

243 above ground level in Qingdao (36.10° N, 120.32° E), using the Hybrid Single-Particle

244 Lagrangian Integrated Trajectory (HYSPLIT) model in the GIS-based software of TrajStat

245 (Wang et al., 2009). The weather data was acquired from Global Data Assimilation System

246 with horizontal resolution of one-degree latitude-longitude (available at

247 http://www.arl.noaa.gov/, last access: 29 October 2021). PSCF was then analyzed based on

248 the trajectories added to source concentrations. The study region was divided into equal-sized

249 grid cells, thus the number of endpoints for given specific values in every cell could be

250 obtained. According to pre-set threshold criterion, the PSCF value was the proportion of the

251 number of endpoints beyond the threshold criterion in each cell. To improve the accuracy of

252 the result, weighted PSCF was calculated. More details are given in Text S3 of supplementary

253 material.

254

3 Results and discussion

3.1 Variation characteristics of the air quality

3.1.1 Trend analysis and annual changes

The annual mean concentration of $PM_{2.5}$ and PM_{10} in Qingdao decreased by 38% and 38% from 51 and 98 $\mu g\ m^{-3}$ in 2015 to 32 and 61 $\mu g\ m^{-3}$ in 2020, respectively. The annual mean $PM_{2.5}/PM_{10}$ was 0.47 $\pm$ 0.02, with little change from 2015 to 2020, suggesting the significant impact of coarse particle sources (e.g. dust) in Qingdao. The annual mean levels of SO_2 and NO_2 declined by 72% and 8% from 27 and 33 $\mu g\ m^{-3}$ in 2015 to 8 and 31 $\mu g\ m^{-3}$ in 2020, respectively. The concentration of SO_2 showed a significant downward trend, while that of NO_2 changed little, probably indicating that the impact of coal-fired sources was significantly reduced, while the impact of mobile sources might still be obvious. The annual mean level of CO decreased by 32% from 0.91 $mg\ m^{-3}$ in 2015 to 0.62 $mg\ m^{-3}$ in 2020, while that of O_3 changed little with ranging from 71 to 69 $\mu g\ m^{-3}$.

In order to shield the impact of meteorological dispersion, the normalized air quality parameters were acquired using the RF algorithm under 30-year average (1990–2020) meteorological conditions. The Theil–Sen trends of air pollutant concentrations after weather normalization by RF modelling are shown in Fig. 1. The decreasing real trend for air pollutants except for O_3 was found after the weather normalization (Fig. 1), indicating that the air quality is gradually improving in Qingdao. The trends of the normalized air quality parameters represent the effects of emission control and, in some cases, associated chemical processes (Vu et al., 2019). The Theil-Sen trend analysis of air pollutant concentrations and $PM_{2.5}/PM_{10}$ and SO_2/NO_2 after the weather normalization is shown in Fig. 1. Compared with other air pollutants, the decline rate of SO_2 concentration was the highest (15.5% yr^{-1}), whereas that of O_3 concentration was the lowest (0.2% yr^{-1}). Note that the decline rate of $PM_{2.5}$ concentration (6.0% yr^{-1}) was higher than that of PM_{10} concentration (5.6% yr^{-1}), which led to a slight downward trend for $PM_{2.5}/PM_{10}$ (0.6% yr^{-1}), indicating that the impact of coarse particle sources such as dust might be prominent. The decline rate of SO_2 concentration was higher than that of NO_2 concentration (1.0% yr^{-1}), resulting in a higher SO_2/NO_2 decline rate of 15.3% yr^{-1}, indicating that the control effect of stationary sources was better than that of mobile sources (Nirel and Dayan, 2001). It was found that CO

285 concentration also performed an obvious decreasing trend, with the decreasing rate reaching

286 5.2% yr^{-1}, whereas the downward trend of O_3 concentration was not prominent. The

287 normalized medians of $PM_{2.5}$, PM_{10}, SO_2, NO_2, CO and O_3 decreased by 2.8, 5.4, 3.4, 0.3,

288 42.8, and 0.1 $\mu g\ m^{-3}\ yr^{-1}$, respectively (Table S7). Similar to this study, Vu et al. (2019) found

289 that primary emission controls required by the CAAP in Beijing have led to substantial

290 reductions in $PM_{2.5}$, $PM_{10,}$ NO_2, SO_2, and CO from 2013 to 2017 of approximately 34%, 24%,

291 17%, 68%, and 33%, respectively, after meteorological normalization. Zhai et al. (2019)

292 suggested that the mean $PM_{2.5}$ decreased across China was 4.6 $\mu g\ m^{-3}\ yr^{-1}$ in the

293 meteorology-corrected data from 2013 to 2018, and the Beijing-Tianjin-Hebei, the Yangtze

294 River Delta, the Pearl River Delta, the Sichuan Basin, and the Fenwei Plain decreased 8.0,

295 6.3, 2.2, 4.9, and 5.0 $\mu g\ m^{-3}\ yr^{-1}$, respectively. Overall, the concentrations of most air

296 pollutants (i.e., $PM_{2.5}$, PM_{10}, SO_2, NO_2, and CO) in China have showed a decreasing trend in

297 recent years (Zhao et al., 2021a; Fan et al., 2020, while that of O_3 has performed an

298 increasing trend (Li et al., 2020a; Ma et al., 2021), which further facilitated secondary

299 particles formation (Wang et al., 2016; Nøjgaard et al., 2012).

300   Figure S3 compares the trends of air pollutants before and after normalization from 2015

301 to 2020, which are largely different depending on meteorological conditions (Vu et al., 2019).

302 The annual average concentrations of $PM_{2.5}$, PM_{10}, SO_2, NO_2, CO, and O_3 after normalization

303 were higher than the actual observed concentrations. Compared with 2018, the observed

304 concentrations of air pollutants in 2019 showed an increase in varying degrees; however, the

305 increasing values of annual average concentrations for $PM_{2.5}$, PM_{10}, SO_2, CO, and O_3 after

306 normalization decreased, and even the NO_2 concentration after normalization also decreased.

307 This indicates that the meteorological conditions in 2019 reduced the effect of actual control

308 to some extent. Up to that point, emission control had resulted in reductions of $PM_{2.5}$, PM_{10},

309 SO_2, NO_2, CO, and O_3 concentrations by 17.7%, 31.9%, 18.4%, 1.7%, 0.3%, and 0.4% from

310 2015 to 2020, respectively, highlighting that much work is still needed to ensure the decrease

311 of NO_2 and O_3 concentrations in the future.

312

313 3.1.2 Changes in the air quality in the two control stages

314   In order to assess the changes in ambient air quality in Qingdao during different policy

315   control periods, this study analyzed the changes in air pollutant concentrations during two

316   stages: the CAAP period (stage 1: 2015-2017) and the BSPC period (stage 2: 2018-2020).

317   The observed annual mean concentrations for $PM_{2.5}$ and PM_{10} during stage 1 were 45 and 89

318   $\mu g\ m^{-3}$, respectively (Table S8), and their annual average decline rates were 11.9% and 8.0%

319   after weather normalization, respectively. Li et al. (2019b) found that $PM_{2.5}$ decreased by 30-

320   40% across China during 2013-2017 in response to the governmental Clean Air Action.

321   Compared with stage 1, the annual average concentrations of $PM_{2.5}$ and PM_{10} observed in

322   stage 2 were 35 and 71 $\mu g\ m^{-3}$, respectively (Table S8), and the decline range after

323   normalization was reduced, with the decline rates of 5.3% and 7.0%, respectively (Fig. 2).

324   However, $PM_{2.5}/PM_{10}$ ratios during two stages were less than 0.5, suggesting that the impact

325   of dust sources might be obvious in the two stages. Note that the mean observed annual

326   concentration of SO_2 was 21 $\mu g\ m^{-3}$ in the stage 1 (Table S8) and its annual average decline

327   rate reached 25.0% after normalization (Fig. 2), which was significantly higher than that of

328   other pollutants. Compared with stage 1, the observed annual average concentration of SO_2 in

329   stage 2 was only 8 $\mu g\ m^{-3}$ (Table S8), and the annual decline rate of SO_2 concentration after

330   normalization still reached 17.1% (Fig. 2), indicating that Qingdao had achieved remarkable

331   results in the control of coal combustion during the two stages. The observed annual mean

332   concentrations for NO_2 and O_3 during stage 1 were 34 and 73 $\mu g\ m^{-3}$, respectively (Table S8),

333   and their annual increasing rates after normalization were 1.5% and 2.8%, respectively (Fig.

334   2). Study showed that surface ozone pollution in China worsened over the stage 1 (Li et al.,

335   2019b). The observed annual mean concentrations of NO_2 and O_3 in stage 2 were 32 and 71

336   $\mu g\ m^{-3}$, respectively (Table S8), while their annual decline rates after normalization were only

337   2.7% and 2.0%, respectively (Fig. 2). This indicates that the impact of motor vehicles in

338   Qingdao could be greater than expected. Meanwhile, NO_2 and volatile organic compounds

339   emitted from motor vehicles are important precursors for the formation of O_3 (Pugliese et al.,

340   2014; Tsai et al., 2010), which were found to have further enhanced the O_3 concentration in

341   Qingdao's atmosphere. The mean observed annual concentrations for CO were 0.80 and 0.64

342   $mg\ m^{-3}$ in stages 1 and 2, respectively (Table S8), and the annual average decline rate were

343   11.4% and 3.2% after normalization, respectively (Fig. 2), suggesting that there might have

344   been a benefit from the significant control effect of coal-fired sources.

345   Diurnal variations of concentrations of air pollutants and $PM_{2.5}/PM_{10}$ and SO_2/NO_2

346   after normalization in the two stages are shown in Fig. S4. The diurnal variation in $PM_{2.5}$

347   concentration in the two stages was basically the same; however, the concentration of $PM_{2.5}$

348   in stage 2 was significantly lower than that in stage 1. Diurnal variation of PM_{10}

349   concentration in the two stages was similar to $PM_{2.5}$. The daily variations of $PM_{2.5}/PM_{10}$ in

350   the two stages were basically the same, and the $PM_{2.5}/PM_{10}$ between 06:00-20:00 in stage 2

351   was slightly lower than that in stage 1, probably suggesting that the impact of dust increased

352   slightly during this period. The diurnal variations of SO_2 and CO concentrations during

353   stages 1 and 2 were generally consistent, whereas their concentrations in stage 2 were

354   substantially lower than those in stage 1, which might indicate that the control effects of coal

355   combustion in Qingdao in stage 2 was obvious. In contrast, the diurnal variations of NO_2

356   concentrations in stages 1 and 2 were basically consistent with the values at each time,

357   suggesting that the impact of motor vehicles in Qingdao might still be significant, especially

358   the morning and evening peaks and between 21:00 and 23:00 at night. The daily variations of

359   O_3 concentrations were highly consistent in the two stages, especially between 14:00 and

360   17:00, O_3 pollution was still severe. In general, compared with stage 1, the concentrations of

361    $PM_{2.5}$, PM_{10}, SO_2, and CO in stage 2 decreased remarkably at all times, while those of NO_2

362   and O_3 remained basically unchanged at all times, indicating that the control effect of coal-

363   fired sources in Qingdao was significant, whereas the impact of motor vehicles and O_3

364   pollution were more obvious.

365

366   3.1.3 Changes in air quality after the COVID-19 lockdown

367   In response to the COVID-19 outbreak, a series of lockdown measures were

368   implemented in China to curb the virus transmission, resulting in a significant decrease in

369   traffic and industrial activities. These limitations provided an opportunity to investigate

370   critical pollution sources that could potentially be better managed in the future to further

371   improve the air quality. In order to explore the changes of air quality in Qingdao during the

372   COVID-19 lockdown period, combined with the specific lockdown situation of Qingdao

373   (http://wsjkw.shandong.gov.cn/ywdt/xwtt/202001/t20200124_3420319.html;

374   http://www.shandong.gov.cn/art/2020/3/7/art_119816_350607.html; last access: 29 October

375   2021), this study divided the lockdown period into three stages: pre-lockdown (1 to 24

376   January, 2020), full lockdown (25 January to 7 March, 2020), and partial lockdown (8 to 31

377   March, 2020). The time series and average values of air pollutant concentrations and

378    $PM_{2.5}/PM_{10}$ and SO_2/NO_2 during different lockdown stages and their corresponding periods

379   in 2018 and 2019 are shown in Fig. 3 and Tables S9-S10. According to the weather

380   normalization data, compared with that before the lockdown, the concentrations of $PM_{2.5}$,

381   PM_{10}, SO_2, NO_2, and CO decreased substantially during the full lockdown, among which the

382   concentrations of PM_{10} and NO_2 decreased the most (49.5% and 49.0%, respectively),

383   followed by $PM_{2.5}$ (47.8%) (Table S11), which was closely related to the significant decrease

384   in traffic and construction activities during the full lockdown (Collivignarelli et al. 2021;

385   Hong et al. 2021; Wang et al. 2021a). Note that the O_3 concentration increased apparently by

386   50.8% during the full lockdown (Table S11), suggesting that the atmospheric oxidation might

387   be enhanced during this period, similar to the study of Chu et al. (2021), Ding et al., (2021),

388   He et al., (2020), and Le et al. (2020). PM_{10} and NO_2 concentrations rebounded significantly

389   during partial lockdown, increasing by 20.3% and 21.1% compared with the full lockdown,

390   respectively, likely due to the increased impacts of traffic activities and related road dust. The

391   concentrations of $PM_{2.5}$, SO_2, and CO further decreased during the partial lockdown. The

392   study from Yin et al. (2021) showed that the decrease of $PM_{2.5}$ concentration might be mainly

393   due to the meteorological conditions.

394   Compared with the same period in 2018, the concentrations of $PM_{2.5}$, PM_{10}, SO_2, NO_2,

395   CO, and O_3 decreased obviously during the full lockdown, of which the reduction range of

396   SO_2 concentration was the greatest (39.8%), whereas that of O_3 concentration was relatively

397   lowest (1.8%) (Table S12). Compared with the corresponding period in 2019, the

398   concentrations of $PM_{2.5}$, PM_{10}, SO_2, NO_2, and CO decreased by 34.5%, 44.8%, 27.0%, 32.6%,

399   and 22.3% during the full lockdown, respectively, while that of O_3 increased by 3.9% (Table

400   S12). This shows that the COVID-19 lockdown measures led to the marked decrease of the

401   primary emissions of air pollutants. Meanwhile, the concentrations of particulate matter and

402   NO_2 decreased substantially during the full lockdown. Since there are relatively few

403   industrial enterprises in urban area of Qingdao, NO_2 is mainly emitted from motor-vehicles.

404   Therefore, this suggested that the control of motor-vehicles under normal conditions should

405   play an important role in the improvement of air quality in Qingdao.

406

407   **3.2 Changes in meteorological conditions and chemical compositions**

408   In this study, the VC in the same period was used to normalize the concentrations of

409   chemical compositions in $PM_{2.5}$. After reducing the impacts of meteorological dispersion, the

410   changes in the concentrations of major chemical compositions in the different years were

411   analyzed to better reflect the impacts of source emissions (Dai et al., 2020; Ding et al., 2021).

412   In 2011-2012, 2016, and 2019, the annual average MLHs in Qingdao were 399, 383, and 414

413   m, respectively (Fig. S5). However, the average wind speed in 2016 was significantly higher

414   than that in other years, reaching 3.3 m s^{-1}. The VC showed an increasing trend year by year,

415   from 1292.7 to 1555.4 m s^{-2} (Fig. S5), suggesting that the atmospheric dispersion conditions

416   in Qingdao were gradually increasing. The average VC of Qingdao in three years was 1432.6

417   m s^{-2}, and higher MLH usual corresponds to higher wind speed. Time series of observed

418   concentrations and normalized concentrations of $PM_{2.5}$ and chemical compositions are shown

419   in Fig. S6. The observed and VC normalized concentrations of $PM_{2.5}$ during the whole study

420   period were 93 and 83 μg m^{-3}, respectively, suggesting that the unfavorable meteorological

421   conditions might increase approximately 10 μg m^{-3} of $PM_{2.5}$, which was substantially lower

422   than that reported by the study of Ding et al. (2021) in Tianjin. Zhai et al. (2019) found that

423   the mean $PM_{2.5}$ in the meteorology-corrected data from 2013 to 2018 was 12% lower than in

424   the original data, meaning that 12% of the $PM_{2.5}$ decrease in the original data was attributable

425   to the meteorology. However, Gong et al. (2022) suggested that the meteorology can explain

426   approximately 20-33% of the $PM_{2.5}$ variations.

427   The annual changes in the observed and dispersion normalized concentrations and

428   percentages of main chemical compositions in ambient $PM_{2.5}$ are shown in Fig. 4 and Fig. S7.

429   From 2011-2012 to 2019, the observed concentrations of SO_4^{2-} showed an obvious downward

430   trend, from 23.5 to 6.7 μg m^{-3}. The trend of concentrations of SO_4^{2-} after dispersion

431   normalization was consistent with the observed concentrations, and the annual average

432   decline rate was approximately 41.5% (38.1% in 2016 and 44.8% in 2019) (Table S13),

433   probably suggesting that the impacts of coal-fired sources in Qingdao has decreased

434   substantially in recent years. In contrast, the observed concentrations and percentages of NO_3^-

435 increased significantly from 2011-2012 (3.5 µg m^{-3}) to 2019 (10.0 µg m^{-3}), and NO$_3^-$/SO$_4^{2-}$

436 increased from 0.14 to 1.50. After dispersion normalization, the concentrations and

437 percentages of NO$_3^-$ changed inappreciable in 2016-2019 but significantly higher than that

438 prior to the CAAP. It has been found that ambient NO$_3^-$ in urban mainly originates from the

439 secondary conversion of NOx emitted by motor-vehicles (Alexander et al., 2020; Liu et al.,

440 2017; Meng et al., 2008), thereby indicating that the impacts of motor-vehicles in Qingdao

441 might become increasingly obvious. The observed and normalized concentrations and

442 percentages of OC and EC basically performed a downward trend from 2011 to 2019. The

443 OC concentration decreased significantly, and the observed and normalized concentrations

444 decreased from 13.1 to 7.6 µg m^{-3} and 12.9 to 7.2 µg m^{-3}, respectively, which might be related

445 to the significant decrease in the impacts of coal-fired sources in Qingdao. Note that the

446 annual variations of observed and normalized concentrations of NH$_4^+$ were consistent with

447 that of SO$_4^{2-}$, but contrary to that of NO$_3^-$, which might indicate that ammonium mainly

448 existed in the form of ammonium sulfate and ammonia hydrogen sulfate in Qingdao.

449   Crustal elements (Si, Al, and Mg) decreased remarkably after the CAAP were in place.

450 The observed and normalized concentrations of these elements in 2011-2012 were higher

451 than those in 2016 and 2019, while their concentrations in 2019 were slightly higher than

452 those in 2016. From 2011-2012 to 2019, the observed concentrations of Si, Al, and Mg

453 decreased from 10.7 to 1.0 µg m^{-3}, 3.1 to 0.5 µg m^{-3}, and 1.9 to 0.2 µg m^{-3}, respectively, and

454 the trends of normalized concentrations were consistent with the observed concentrations,

455 likely suggesting that the impact of dust in 2011-2012 was apparently higher than that in

456 2016 and 2019, and 2019 rebounded compared with 2016. The trends of the observed and

457 normalized concentrations and percentages of Ca were consistent. The concentrations and

458 percentages in 2011-2012 were remarkedly higher than that in 2016 and 2019, and the

459 concentration in 2019 rebounds compared with that in 2016, with the increasing rate of 77.1%

460 in terms of normalized data (Table S13). This suggests that the impact of construction

461 activities in 2011-2012 might have been significantly higher than that in 2016 or 2019. The

462 annual trends of observed and normalized concentrations of Fe were also consistent. The

463 observed and normalized concentrations in 2011-2012 were 4.0 and 4.6 µg m^{-3}, respectively.

464 After 2016, the concentrations and percentages of Fe decreased substantially, which might be

465 closely related to the relocation of iron and steel enterprises in Qingdao (Liu et al., 2021a).

466 The observed and normalized concentrations and percentages of Ni and V basically showed a

467 downward trend from 2011-2012 to 2019. The concentrations in 2011-2012 were

468 significantly higher than that in 2016 and 2019, which might indicate that the impact from

469 ships in 2011-2012 was more obvious. Of course, it might also be related to the impact of

470 manual dust sources. From 2011-2012 to 2019, the observed and normalized concentrations

471 and percentages of Na showed a downward trend. The concentration and percentage in 2011-

472 2012 were significantly higher than those in 2016 and 2019, suggesting that the impact of sea

473 salt might have decreased in Qingdao in recent years.

474

475 **3.3 Changes in source contributions**

476 3.3.1 Source identification

477   Given that the differences of source profiles during different periods, PMF analysis was

478 conducted for three data sets corresponding to separate sampling periods (i.e., 2011-2012,

479 2016, and 2019). The solutions from five to nine factors were examined in terms of scaled

480 residuals, factor interpretability, and displacement acceptability (Brown et al., 2015; Dai et al.,

481 2020). An eight-factor solution was chosen as the optimal fits for each data set. The

482 correlation coefficients (R^2) between the observed and calculated concentrations were 0.91,

483 0.83, and 0.91, respectively (Fig. S8). There were no DISP swaps, and all BS runs had at least

484 87% agreement with the base case values (Table S14).

485   The factor profiles estimated from PMF during different periods are shown in Figs. S9-

486 S11. The first factor was identified as vehicle emissions, because OC and EC both had high

487 concentrations and explained variations as well as narrow DISP bounds. It is known that the

488 OC and EC are important tracers for vehicle emissions (Bi et al., 2019; Gao et al., 2016;

489 Ryou et al., 2018; Xu et al., 2019a). The second factor was characterized by higher

490 concentration and explained variation of Si, and high Al concentrations, and they all had

491 narrow DISP ranges. Si and Al were the indicators for fugitive dust (Begum et al., 2011; Jain

492 et al., 2018; Zhao et al., 2021b). The third factor featured relatively high concentrations and

493 explained variations of OC, SO_4^{2-}, and Cl^- with tight DISP intervals. These species were

494 distinctive tracers for coal combustion (Huang et al., 2017; Song et al., 2021; Tao et al., 2014).

495   The fourth factor was characterized by high explained variations of Fe and Mn, and

496   relatively high concentrations of Cu and Zn. Tsai et al. (2020) found that Fe and Mn were

497   related to basic oxygen, iron ore sintering and steel oxidation refining. Querol et al. (2007)

498   and Kuo et al. (2007) have reported that Cu and Zn were released from multiple metal

499   smelting. Therefore, this factor was identified as steel-related smelting. The fifth factor was

500   dominated by high concentrations and explained variations of NO_3^- and NH_4^+ with small

501   DISP bounds, which was identified as secondary nitrate (Esmaeilirad et al., 2020). It was

502   found that SO_4^{2-} and NH_4^+ presented the highest explained variations and concentrations with

503   narrow DISP bounds in the sixth factor. Therefore, this factor was assigned as secondary

504   sulphate (Bove et al., 2016; Jain et al., 2020). The seventh factor was featured by high

505   concentration and explained variation of Ca with a small DISP bound, which was identified

506   as construction dust (Liu et al., 2016; Zhang et al., 2005). The final factor was characterized

507   by highly explained variations of Na, Ni, and V with narrow DISP intervals. In addition, the

508   concentrations of Mg, NO_3^-, SO_4^{2-}, and Cl^- in this factor were also relatively high. Zhang et al.

509   (2021), Liu et al. (2018b), Choi et al. (2013), and Police et al. (2016) have found that sea salt

510   involves high amounts of Na, Mg, NO_3^-, SO_4^{2-}, and Cl^-. Meanwhile, Ni and V are the markers

511   of ship emissions (Manousakas et al., 2017; Zong et al., 2018; Xu et al., 2018). Therefore,

512   this factor was recognized as a mixed source of sea salt and ship emissions.

513

514   3.3.2 Change in source contributions

515   The source apportionment results of ambient $PM_{2.5}$ in Qingdao from 2011-2012 to

516   2019 are shown in Fig. 5 and Figs. S12-S15. For vehicle emissions, its contribution showed

517   an increasing trend with each year, from 12.1 µg m^{-3} (7.9%) to 13.6 µg m^{-3} (22.5%). The

518   contribution of coal combustion performed a significant downward trend, from 21.3 µg m^{-3}

519   (13.9%) in 2011-2012 to 4.5 µg m^{-3} (7.5%) in 2019. The contribution of fugitive dust in 2011-

520   2012 was up to 35.3 µg m^{-3} (23.1%), significantly higher than 8.5 µg m^{-3} (13.2%) in 2016 and

521   10.2 µg m^{-3} (16.8%) in 2019, and the contribution in 2019 rebounded compared with 2016.

522   The contribution of construction dust showed a downward trend year after year, from 14.2 µg

523   m^{-3} (9.3%) in 2011-2012 to 2.4 µg m^{-3} (4.0%) in 2019. The contribution of steel-related

524   smelting also showed a downward trend year by year, from 15.9 µg m^{-3} (10.4%) in 2011-

525 2012 to 3.0 μg m^{-3} (4.9%) in 2019. The significant decline in the impact of steel-related

526 smelting after 2016 might be closely related to the relocation of iron and steel enterprises in

527 Qingdao (Liu et al., 2021a). The contribution of secondary nitrate basically performed a

528 significant upward trend, increasing from 14.5 μg m^{-3} (9.5%) in 2011-2012 to 15.2 μg m^{-3}

529 (25.2%) in 2019, which might be related to the high concentration of precursor (NO_2) (Fig. 1)

530 and the increase in atmospheric oxidation in recent years (Chen et al., 2020c; Fu et al., 2020).

531 In contrast, the contribution of secondary sulphate showed a significant downward trend,

532 from 34.2 μg m^{-3} (22.3%) in 2011-2012 to 9.7 μg m^{-3} (16.0%) in 2019, likely due to the

533 significant decrease in the concentration of its precursor (SO_2) (Fig. 1). For sea salt and ship

534 emissions, the contribution basically performed a downward trend, from 5.7 μg m^{-3} (3.7%) in

535 2011-2012 to 2.0 μg m^{-3} (3.2%) in 2019.

536   To shield the impact of meteorology on the source apportionment results, this study used

537 Eq. (2) to conduct the treatment of dispersion normalization for the source apportionment

538 results, and then analyzed the annual changes in the contributions of different source

539 categories, as shown in Fig. S16. The annual changes in the contributions of multiple sources

540 in Qingdao were basically consistent with the results of direct PMF calculation. The

541 contribution of vehicle emissions was increasing year by year, and the annual average

542 increase rate of contribution concentration was 12.1%. However, the contribution of coal

543 combustion showed a continuous yearly downward trend, with the average annual decline

544 rate of contribution concentration being 56.8%. For fugitive dust, compared with 2011-2012,

545 the contribution in 2016 decreased substantially, with a decline rate of contribution

546 concentration of 68.9%, while it rebounded in 2019, with an increase rate of 25.2%. The

547 contribution of construction dust performed a continuous yearly downward trend, with the

548 average annual decline rate of contribution concentration being 55.9%. For the steel-related

549 smelting, and sea salt and ship emissions, the average annual decline rates of their

550 contribution concentrations were 55.3% and 46.0%, respectively. In contrast, the contribution

551 of secondary nitrate showed an increasing trend, and the increase rate of its contribution

552 concentration was 1.7%, while the contribution proportion increased by more than 70%. The

553 contribution of secondary sulphate showed a continuous yearly downward trend, and the

554 average annual decline rate of contribution concentration was 38.7%. Overall, the impacts of

555 coal combustion and steel-related smelting industrial sources in Qingdao decreased

556 substantially over the last decade, suggesting that the controlling effects of these sources were

557 obvious. The impact of motor-vehicles was prominent each year. Qingdao also risks increased

558 emissions from the increased vehicular population and ozone pollution that facilitate

559 secondary particles formation in the future. The impact of fugitive dust had decreased in

560 recent years, whereas its contribution was still obvious. Therefore, the control of motor-

561 vehicles and dust should be the focus of pollution source control in Qingdao in the future,

562 while that of coal combustion and industrial sources also should not be ignored.

563 Furthermore, with the beginning of heating season in northern cities in China (Liu et

564 al., 2016; Li et al., 2019a), the atmospheric pollutant emissions increased substantially (Chen

565 et al., 2020a). Coupled with the adverse meteorological conditions (Li et al., 2019a), haze

566 episodes occurred frequently during this period (Liu et al., 2018a; Yang et al., 2020).

567 Therefore, the control effects of pollution sources and key control sources in the specific

568 period can be better highlighted through analyzing the changes in the contributions of

569 emission sources during heating seasons over the years. In this study, the heating season in

570 2011-2012 was defined from 15 to 29 February, 2012, that in 2016 was defined from 17 to 20

571 December, 2016, and that in 2019 referred from 12 to 26 January, 2019. The contributions of

572 different sources during different heating seasons in Qingdao are shown in Figs. S17-S18.

573 Compared with the heating season in 2011-2012, the contribution of coal combustion

574 decreased significantly in the heating seasons of 2016 and 2019, from 50.2 $\mu g\ m^{-3}$ (31.7%) to

575 10.9 $\mu g\ m^{-3}$ (6.4%) and 10.6 $\mu g\ m^{-3}$ (10.8%). The contribution percentages after dispersion

576 normalization showed a consistent trend. For vehicle emissions, the contribution percentages

577 in the heating season increased continuously each year, from 3.9% in 2022-2012 to 22.3% in

578 2019. The results after normalization had the same trend, suggesting that the impact of motor

579 vehicles in heating season was gradually prominent. The contribution of fugitive dust in the

580 heating season in 2011-2012 (14.2 $\mu g\ m^{-3}$) was substantially higher than that in 2016 (3.9 μg

581 m^{-3}) and 2019 (12.0 $\mu g\ m^{-3}$). The contribution in the heating season in 2019 rebounded

582 remarkably compared with that in 2016, and the results of dispersion normalization were

583 consistent. The contribution of construction dust in the heating season in 2019 was markedly

584 lower than that in 2011-2012 and 2016. The contribution of steel-related smelting in the

585 heating season showed a continuous yearly downward trend, from 22.6 μg m^{-3} in the heating

586 season from 2011-2012 to 4.6 μg m^{-3} in 2019. However, its contribution percentage in the

587 heating season in 2019 was higher than that in the heating season in 2016, which was

588 consistent with the normalized results, indicating that the impact of steel-related smelting in

589 the heating season had increased, though the contribution percentage was low. The

590 contribution of secondary nitrate in heating season in 2016 was up to 61.3 μg m^{-3} (36.3%),

591 which was significantly higher than that of 28.4 μg m^{-3} (28.9%) in 2019 and 16.8 μg m^{-3}

592 (10.6%) in 2011-2012. This was consistent with the results of the dispersion normalization. It

593 can be seen that although the contribution of secondary nitrate in the heating season in 2019

594 was reduced, its contribution was significantly higher than that of other sources. Similarly,

595 the contribution of secondary sulphate was also higher in the heating season of 2016 than

596 other years; however, its contribution was clearly lower than that of secondary nitrate. After

597 dispersion normalization, the contributions of secondary sulphate basically showed a

598 continuous yearly downward trend. The contribution of sea salt and ship emissions in the

599 heating season also showed an obvious downward trend, from 10.0 μg m^{-3} (6.3%) in 2011-

600 2012 to 1.4 μg m^{-3} (1.5%) in 2019, and the results after dispersion normalization were

601 basically consistent. The average decline rate of contribution concentration was

602 approximately 70%, including 88% in 2016. From this analysis, the impacts of coal

603 combustion and steel-related smelting in Qingdao were relatively low after the heating season

604 in 2016, while that of vehicle emissions was prominent each year. Although the impact of

605 fugitive dust had rebounded in the heating season in 2019, the contribution was relatively low.

606 The contribution of secondary nitrate in heating season was substantially higher than that of

607 other sources, and the influence of secondary sulfate decreased each year. The influence of

608 sea salt and ship emissions in heating season showed a continuous yearly downward trend.

609

610 **3.4 Changes in potential source areas**

611   Similar to the studies of Liu et al. (2021a) and Dai et al. (2020), according to the source

612 apportionment results, this study used the PSCF method to analyze the changes in the

613 potential impact areas of emission sources in Qingdao from 2011-2012 to 2019, and the

614 results are shown in Fig. 6. For vehicle emissions, the potential impact areas changed greatly

from 2011-2012 to 2019. The potential impact areas in 2011-2012 were located at the

junction of Shandong, Henan, Anhui, and Jiangsu provinces, and the potential impact areas

were mainly located in the south part of Jiangsu in 2016, while in 2019, Tianjin and the

northwest part of Shandong were important impact areas. The potential impact areas for

fugitive dust showed a trend of westward migration from 2011-2012 to 2019. For 2011-2012,

the potential impact areas were located at the junction of Shandong, Henan, Anhui, and

Jiangsu, as well as in the northern part of Shandong. The potential impact areas were located

in the northwestern part of Shandong in 2016, while they were at the junction of Shandong

and Henan in 2019. For coal combustion, the potential impact areas for 2011-2012 were

located at the junction of Shandong, Henan, Anhui, and Jiangsu. In 2016, they moved to the

northwest of Shandong Province and Beijing Tianjin and Hebei region, and the northwest of

Shandong was an important impact area in 2019. For steel-related smelting, Beijing and

Tianjin were the potential impact areas for 2011-2012, while the potential impact area was

located in the Yellow Sea in 2016, which might be related to the relocation of iron and steel

enterprises to a port area in the south of Qingdao (Liu et al., 2021a). This suggests that the air

mass transport in the coastal area could lead the nearby sea areas to become potential impact

areas. The potential impact area in 2019 was mainly located at the junction of Hebei, Henan,

and Shandong.

For secondary nitrate, the potential impact area for 2011-2012 was the junction of

Shandong, Henan, Jiangsu, and Anhui provinces. The potential impact area was mainly

located in the central and southern parts of Shandong in 2016, while two areas were located

in Beijing, Tianjin, and the junction of Hebei, Henan, and Shandong provinces in 2019. For

secondary sulphate, the main potential impact areas for 2011-2012 were located at the

junction of Shandong, Henan, Jiangsu, and Anhui Provinces and the western part of Jilin

Province. The impact of the Middle East of Shandong Province was more obvious in 2016,

while the impact was greater in the south part of Shandong Province, and the junction of

Henan and Jiangsu Provinces in 2019. For construction dust, the main potential impact areas

for 2011-2012 were Beijing, Tianjin, and the western part of Shandong Province, and the

southeastern part of Hebei Province, Shanghai, and the eastern part of Hubei Province in

2016, while the central and western parts of Shandong Province, the junction of Henan and

Shandong Provinces, and the central and southern parts of Anhui Province were the main impact areas in 2019. For sea salt and ship emissions, the potential impact areas for 2011-2012 were mainly located in coastal areas of Jiangsu and Shanghai, which were closely related to the impacts of ship emissions from ports and sea salt in these cities. The Yellow Sea was the main impact area in 2016 and 2019, and the impact areas in 2019 moved to the south. Bie et al. (2021) also analyzed the potential impact areas of ship emissions in Qingdao Port from 2018 to 2019 using the PSCF method, and found that they were mainly located in the Bohai Bay, Yellow Sea, and Yangtze River Delta. Overall, from 2011-2012 to 2019, the potential impact areas of different emission sources in Qingdao have changed markedly. In 2019, the potential impact areas for most of the emission sources were mainly located in Shandong Province and along the border areas between the western or southwest parts of Shandong and other provinces, while sea salt and ship emissions were mainly affected by transport on the Yellow Sea.

4 Conclusions

A machine learning-based meteorological normalization and a dispersion normalization-based on ventilation coefficient approaches were applied to decouple the meteorological deduced variations in air quality time series and multiple source contributions of a coastal city in northern China (Qingdao), respectively. The concentrations of air pollutants other than ozone in Qingdao decreased substantially and the air quality improved continuously after the "CAAP" period, indicating that the control strategies of air pollution in Qingdao over the years have been proper. The largest emission reduction sections were likely from coal combustions and industrial emissions from 2011-2012 to 2019, and the decrease of steel-related smelting after 2016 due to the relocation of iron and steel enterprises. The contribution of dust in Qingdao decreased remarkably after the "CAAP", but the impact was still outstanding until 2019. Vehicle emissions were increased in importance, as opposed to the other primary sources. Qingdao risks increased emissions from the increased vehicular population and ozone pollution that facilitate secondary particles formation in the future. In addition, the influence of ship emissions should be gradually reduced. The control of motor-vehicles and dust should be the focus of pollution source control in Qingdao in the future,

675 while that of coal combustion and industrial sources cannot be ignored. In addition, the

676 potential impact areas of different emission sources in Qingdao have changed markedly from

677 2011-2012 to 2019. The potential impact areas for most of emission sources were mainly

678 located in Shandong and the border areas between western or southwest Shandong and other

679 provinces in 2019, while sea salt and ship emissions were mainly affected from the transport

680 of the Yellow Sea.

681

682 **Author contributions**

683 Baoshuang Liu: Data curation, Writing – original draft, Yanyang Wang: Data curation and

684 Investigation, He Meng: Data collection, Qili, Dai: Supervision and Review, Liuli Diao: Data

685 curation, Jianhui Wu: Supervision, Laiyuan Shi: Supervision, Jing Wang: Supervision, Yufen

686 Zhang: Supervision – review & editing, Yinchang Feng: Supervision – review & editing.

687 **Competing interests**

688 The authors declare no competing financial interests.

689 **Acknowledgements**

690 The authors are grateful to the Qingdao Eco-environment Monitoring Center of Shandong

691 Province for collection of particulate matter samples in this study.

692 **Financial support**

693 This study was financially supported by the National Research Program for Key Issues in Air

694 Pollution Control (No. DQGG2021301), the Tianjin Science and Technology Plan Project

695 (No. PTZWHZ00120) and the Fundamental Research Funds for the Central Universities:

696 Nankai University (No. 63211074).

697

698 **References**

699 Alexander, B., Sherwen, T., Holmes, C. D., Fisher, J. A., Chen, Q., Evans, M. J., and Kasibhatla, P.: Global
700   inorganic nitrate production mechanisms: comparison of a global model with nitrate isotope
701   observations, Atmos. Chem. Phys., 20, 3859-3877, https://doi.org/10.5194/acp-2019-422, 2020.
702 Begum, B. A., Biswas, S. K., and Hopke, P. K.: Key issues in controlling air pollutants in Dhaka,
703   Bangladesh, Atmos. Environ., 45, 7705-7713, https://doi.org/10.1016/j.atmosenv.2010.10.022, 2011.
704 Beloconi, A., Probst-Hensch, N. M., and Vounatsou, P.: Spatio-temporal modelling of changes in air
705   pollution exposure associated to the COVID-19 lockdown measures across Europe, Sci. Total
706   Environ., 787, 147607, https://doi.org/10.1016/j.scitotenv.2021.147607, 2021.
707 Bi, X. H., Dai, Q. L., Wu, J. H., Zhang, Q., Zhang, W. H., Luo, R. X., Cheng, Y., Zhang, J. Y., Wang, L., Yu,

Z. J., Zhang, Y. F., Tian, Y. Z., and Feng, Y. C.: Characteristics of the main primary source profiles of particulate matter across China from 1987 to 2017, Atmos. Chem. Phys., 19, 3223-3243, https://doi.org/10.5194/acp-19-3223-2019, 2019.

Bie, S. J., Yang, L. X., Zhang, Y., Huang, Q., Li, J. S., Zhao, T., Zhang, X. F., Wang, P. C., and Wang, W. X.: 2021. Source appointment of $PM_{2.5}$ in Qingdao Port, East of China, Sci. Total Environ., 755, 142456, https://doi.org/10.1016/j.scitotenv.2020.142456, 2021.

Bove, M. C., Brotto, P., Calzolai, G., Cassola, F., Cavalli, F., Fermo, P., Hjorth, J., Massabò, D., Nava, S., Piazzalunga, A., Schembari, C., and Prati, P.: PM_{10} source apportionment applying PMF and chemical tracer analysis to ship-borne measurements in the Western Mediterranean, Atmos. Environ., 125, 140-151, https://doi.org/10.1016/j.atmosenv.2015.11.009, 2016.

Brown, S. G., Eberly, S., Paatero, P., and Norris, G. A.: Methods for estimating uncertainty in PMF solutions: Examples with ambient air and water quality data and guidance on reporting PMF results, Sci. Total Environ., 518, 626-635, https://doi.org/10.1016/j.scitotenv.2015.01.022, 2015.

Chen, J. Y., Shan, M., Xia, J. J., and Jiang, Y.: Effects of space heating on the pollutant emission intensities in "2+26" cities, Building Environ., 175, 106817, https://doi.org/10.1016/j.buildenv.2020.106817, 2020a.

Chen, Y., Zhang, S. M., Peng, C., Shi, G. M., Tian, M., Huang, R. J., Guo, D. M., Wang, H. B., Yao, X. J., Yang, F. M.: Impact of the COVID-19 pandemic and control measures on air quality and aerosol light absorption in Southwestern China, Sci. Total Environ., 749, 141419, https://doi.org/10.1016/j.scitotenv.2020.141419, 2020b.

Chen, X., Wang, H., Lu, K., Li, C., Zhai, T., Tan, Z., Ma, X.,Yang, X., Liu, Y., Chen, S., Dong, H., Li, X., Wu, Z., Hu, M., Zeng, L., and Zhang, Y.: Field Determination of Nitrate Formation Pathway in Winter Beijing, Environ. Sci. Technol., 54, 9243–9253, https://doi.org/10.1021/acs.est.0c00972, 2020c.

Cheng, N. L., Cheng, B. F., Li, S. S., and Ning, T. Z.: Effects of meteorology and emission reduction measures on air pollution in Beijing during heating seasons, Atmos. Pollut. Res., 10, 971-979, https://doi.org/10.1016/j.apr.2019.01.005, 2019.

Choi, J. -K., Heo, J. -B., Ban, S. -J., Yi, S. -M., and Zoh, K. -D.: Source apportionment of $PM_{2.5}$ at the coastal area in Korea, Sci. Total Environ., 447, 370-380, https://doi.org/10.1016/j.scitotenv.2012.12.047, 2013.

Collivignarelli, M. C., De Rose, C., Abbà, A., Baldi, M., Bertanza, G., Pedrazzani, R., Sorlini, S., and Carnevale Miino, M.: Analysis of lockdown for COVID-19 impact on NO_2 in London, Milan and Paris: What lesson can be learnt? Process Saf. Environ. Prot., 146, 952-960 https://doi.org/10.1016/j.psep.2020.12.029, 2021.

Chu, B. W., Zhang, S. P., Liu, J., Ma, Q. X., and He, H.: Significant concurrent decrease in $PM_{2.5}$ and NO_2 concentrations in China during COVID-19 epidemic, J. Environ. Sci., 99, 346-353, https://doi.org/10.1016/j.jes.2020.06.031, 2021.

Carslaw, D. C.: Worldmet: Import Surface Meteorological Data from NOAA Integrated Surface Database (ISD), available at: http://github.com/davidcarslaw/ (last access: 5 September 2018), 2017.

Cohen, A. J., Brauer, M., Burnett, R., Anderson, H. R., Frostad, J., Estep, K., Balakrishnan, K., Brunekreef, B., Dandona, L., Dandona, R., Feigin, V., Freedman, G., Hubbell, B., Jobling, A., Kan, H., Knibbs, L., Liu, Y., Martin, R., Morawska, L., Pope, C. A., Shin, H., Straif, K., Shaddick, G., Thomas, M., van Dingenen, R., van Donkelaar, A., Vos, T., Murray, C. J. L., and Forouzanfar, M. H.: Estimates and 25-year trends of the global burden of disease attributable to ambient air pollution: an analysis of data from the Global Burden of Diseases Study 2015, The Lancet., 389, 1907-1918,

https://doi.org/10.1016/S0140-6736(17)30505-6, 2017.

Cucciniello, R., Raia, L., and Vasca, E.: Air quality evaluation during COVID-19 in Southern Italy: the case study of Avellino city, Environ. Res., 203, 111803, https://doi.org/10.1016/j.envres.2021.111803, 2022.

Dai, Q. L., Liu, B. S., Bi, X. H., Wu, J. H., Liang, D. N., Zhang, Y. F., Feng, Y. C., and Hopke, P. K.: Dispersion Normalized PMF Provides Insights into the Significant Changes in Source Contributions to $PM_{2.5}$ after the COVID-19 Outbreak, Environ. Sci. Technol., 54, 9917-9927, https://doi.org/10.1021/acs.est.0c02776, 2020.

Dai, Q. L., Ding, J., Hou, L. L., Li, L. X., Cai, Z. Y., Liu, B. S., Song, C. B., Bi, X. H., Wu, J. H., Zhang, Y. F., Feng, Y. C., and Hopke, P. K.: Haze episodes before and during the COVID-19 shutdown in Tianjin, China: Contribution of fireworks and residential burning, Environ. Pollut., 286, 117252, https://doi.org/10.1016/j.envpol.2021.117252, 2021.

Ding, J., Dai, Q. L., Li, Y. F., Han, S. Q., Zhang, Y. F., and Feng, Y. C.: Impact of meteorological condition changes on air quality and particulate chemical composition during the COVID-19 lockdown, J. Environ. Sci., 109, 45-56, https://doi.org/10.1016/j.jes.2021.02.022, 2021.

Esmaeilirad, S., Lai, A., Abbaszade, G., Schnelle-Kreis, J., Zimmermann, R., Uzu, G., Daellenbach, K., Canonaco, F., Hassankhany, H., Arhami, M., Baltensperger, U., Prévôt, A. S. H., Schauer, J. J., Jaffrezo, J. -L., Hosseini, V., and El Haddad, I.: Source apportionment of fine particulate matter in a Middle Eastern Metropolis, Tehran-Iran, using PMF with organic and inorganic markers, Sci. Total Environ., 705, 135330, https://doi.org/10.1016/j.scitotenv.2019.135330, 2020.

Fan, H., Zhao, C. F., and Yang, Y. K.: A comprehensive analysis of the spatio-temporal variation of urban air pollution in China during 2014–2018, Atmos. Environ., 220, 117066, https://doi.org/10.1016/j.atmosenv.2019.117066, 2020.

Fu, X., Wang, T., Gao, J., Wang, P., Liu, Y. M., Wang, S. X., Zhao, B., and Xue, L. K.: Persistent Heavy Winter Nitrate Pollution Driven by Increased Photochemical Oxidants in Northern China, Environ. Sci. Technol., 54, 3881–3889, https://doi.org/10.1021/acs.est.9b07248, 2020.

Gao, J., Peng, X., Chen, G., Xu, J., Shi, G. L., Zhang, Y. C., and Feng, Y. C.: Insights into the chemical characterization and sources of $PM_{2.5}$ in Beijing at a 1-h time resolution, Sci. Total Environ., 542, 162-171, https://doi.org/10.1016/j.scitotenv.2015.10.082, 2016.

Gao, Y., Shan, H. Y., Zhang, S. Q., Sheng, L. F., Li, J. P., Zhang, J. X., Ma, M. C., Meng, H., Luo, K., Gao, H. W., and Yao, X. H.: Characteristics and sources of $PM_{2.5}$ with focus on two severe pollution events in a coastal city of Qingdao, China, Chemosphere, 247, 125861, https://doi.org/10.1016/j.chemosphere.2020.125861, 2020.

Grange, S. K., Carslaw, D. C., Lewis, A. C., Boleti, E., and Hueglin, C.: Random forest meteorological normalization models for Swiss PM_{10} trend analysis, Atmos. Chem. Phys., 18, 6223–6239, https://doi.org/10.5194/acp-18-6223-2018, 2018.

Grange, S. K., and Carslaw, D. C.: Using meteorological normalization to detect interventions in air quality time series, Sci. Total Environ., 653, 578–588, https://doi.org/10.1016/j.scitotenv.2018.10.344, 2019.

Gong, S. L., Zhang, L., Liu, C., Lu, S. H., Pan, W. J., and Zhang, Y. H.: Multi-scale analysis of the impacts of meteorology and emissions on $PM_{2.5}$ and O_3 trends at various regions in China from 2013 to 2020 2. Key weather elements and emissions, Sci. Total Environ., 824, 153847, https://doi.org/10.1016/j.scitotenv.2022.153847, 2022.

Gulia, S., Mittal, A., and Khare, M.: Quantitative evaluation of source interventions for urban air quality improvement - A case study of Delhi city, Atmos. Pollut. Res., 9, 577-583,

796   https://doi.org/10.1016/j.apr.2017.12.003, 2018.

797   He, G. J., Pan, Y. H., and Tanaka, T.: The short-term impacts of COVID-19 lockdown on urban air

798   pollution in China, Nat. Sustainability, 3, 1005-1011, https://doi.org/10.1038/s41893-020-0581-y,

799   2020.

800   Huang, H. Y., Liu, B. S., Li, S., Choe, T. -H., Dai, Q. L., Gu, Y., Diao, L. L., Zhang, S. F., Bi, X. H., Luo, Z.

801   W., Lu, M. M., Zhang, Y. F., and Feng, Y. C.: An estimation method for regional transport

802   contributions from emission sources based on a high-mountain site: a case study in Zhumadian, China,

803   Atmos. Environ., 263, 118664, https://doi.org/10.1016/j.atmosenv.2021.118664, 2021.

804   Huang, J., Pan, X. C., Guo, X. B., and Li, G. X.: 2018. Health impact of China's Air Pollution Prevention

805   and Control Action Plan: an analysis of national air quality monitoring and mortality data, The Lancet

806   Planetary Health., 2, e313-e323, https://doi.org/10.1016/S2542-5196(18)30141-4, 2018.

807   Huang, R. J., Zhang, Y. L., Bozzetti, C., Ho, K. F., Cao, J. J., Han, Y. M., Daellenbach, K. R., Slowik, J.

808   G., Platt, S. M., Canonaco, F., Zotter, P., Wolf, R., Pieber, S. M., Bruns, E. A., Crippa, M., Ciarelli,

809   G., Piazzalunga, A., Schwikowski, M., Abbaszade, G., Schnelle-Kreis, J., Zimmermann, R., An, Z.

810   S., Szidat, S., Baltensperger, U., El Haddad, I., and Prevot, A. S. H.: High secondary aerosol

811   contribution to particulate pollution during haze events in China, Nature, 514, 218-222,

812   https://doi.org/10.1038/nature13774, 2014.

813   Huang, X. J., Liu, Z. R., Liu, J. Y., Hu, B., Wen, T. X., Tang, G. Q., Zhang, J. K., Wu, F. K., Ji, D. S., Wang,

814   L. L., and Wang, Y. S.: Chemical characterization and source identification of $PM_{2.5}$ at multiple sites

815   in the Beijing-Tianjin-Hebei region, China, Atmos. Chem. Phys., 17, 12941-12962, 10.5194/acp-17-

816   12941-2017, 2017.

817   Hopke, P. K., Dai, Q. L., Li, L. X., and Feng, Y. C.: Global review of recent source apportionments for

818   airborne particulate matter, Sci. Total Environ., 740, 140091,

819   https://doi.org/10.1016/j.scitotenv.2020.140091, 2020.

820   Hong, Y. W., Xu, X. B., Liao, D., Zheng, R. H., Ji, X. T., Chen, Y. T., Xu, L. L., Li, M. R., Wang, H., Xiao,

821   H., Choi, S. D., Chen, J. S.: Source apportionment of $PM_{2.5}$ and sulfate formation during the COVID-

822   19 lockdown in a coastal city of southeast China, Environ. Pollut., 286, 117577,

823   https://doi.org/10.1016/j.envpol.2021.117577, 2021.

824   Iyer, U. S., and Raj, P. E.: Ventilation coefficient trends in the recent decades over four major Indian

825   metropolitan cities, J. Earth Syst. Sci., 122, 537-549, https://doi.org/10.1007/s12040-013-0270-6,

826   2013.

827   Jain, S., Sharma, S. K., Mandal, T. K., and Saxena, M.: Source apportionment of PM_{10} in Delhi, India

828   using PCA/APCS, UNMIX and PMF, Particuology, 37, 107-118,

829   https://doi.org/10.1016/j.partic.2017.05.009, 2018.

830   Jain, S., Sharma, S. K., Vijayan, N., and Mandal, T. K.: Seasonal characteristics of aerosols ($PM_{2.5}$ and

831   PM_{10}) and their source apportionment using PMF: A four year study over Delhi, India, Environ.

832   Pollut., 262, 114337, https://doi.org/10.1016/j.envpol.2020.114337, 2020.

833   Jiang, X., Li, G. L., and Fu, W.: Government environmental governance, structural adjustment and air

834   quality: A quasi-natural experiment based on the Three-year Action Plan to Win the Blue Sky Defense

835   War, J. Environ. Manage., 277, 111470, https://doi.org/10.1016/j.jenvman.2020.111470, 2021.

836   Joshi, P., Ghosh, S., Dey, S., Dixit, K., Choudhary, R. K., Salve, H. R., and Balakrishnan, K.: Impact of

837   acute exposure to ambient $PM_{2.5}$ on non-trauma all-cause mortality in the megacity Delhi, Atmos.

838   Environ. 259, 118548, https://doi.org/10.1016/j.atmosenv.2021.118548, 2021.

839   Kleinman, M. T., Kneip, T. J., and Eisenbud, M.: Seasonal patterns of airborne particulate concentrations

840   in New York City, Atmos. Environ. (1967), 10, 9-11, https://doi.org/10.1016/0004-6981(76)90252-3,

841   1976.

842 Kuo, S. -C., Hsieh, L. -Y., Tsai, C. -H., and Tsai, Y. I.: Characterization of $PM_{2.5}$ fugitive metal in the

843   workplaces and the surrounding environment of a secondary aluminum smelter, Atmos. Environ., 41,

844   6884-6900, https://doi.org/10.1016/j.atmosenv.2007.04.038, 2007.

845 Le, T. H., Wang, Y., Liu, L., Yang, J. N., Yung, Y. L., Li, G. H., and Seinfeld, J. H.: Unexpected air

846   pollution with marked emission reductions during the COVID-19 outbreak in China, Science, 369,

847   702, https://doi.org/10.1126/science.abb7431, 2020.

848 Li, L.Y., Yan, D.Y., Xu, S. H., Huang, M. L., Wang, X. X., and Xie, S. D.: Characteristics and source

849   distribution of air pollution in winter in Qingdao, eastern China. Environ. Pollut., 224, 44-53,

850   https://doi.org/10.1016/j.envpol.2016.12.037, 2017.

851 Li, H., You, S. J., Zhang, H., Zheng, W. D., and Zou, L. J.: Analysis of the impacts of heating emissions on

852   the environment and human health in North China, J. Clean Prod., 207, 728-742,

853   https://doi.org/10.1016/j.jclepro.2018.10.013, 2019a.

854 Li, K., Jacob, D. J., Liao, H., Zhu, J., Shah, V., Shen, L., Bates, K. H., Zhang, Q., and Zhai, S. X.: A two-

855   pollutant strategy for improving ozone and particulate air quality in China, Nat. Geosci., 12, 906-910,

856   https://doi.org/10.1038/s41561-019-0464-x, 2019b.

857 Li, K., Jacob, D. J., Shen, L., Lu, X., De Smedt, I., and Liao, H.: Increases in surface ozone pollution in

858   China from 2013 to 2019: anthropogenic and meteorological influences, Atmos. Chem. Phys., 20,

859   11423-11433, https://doi.org/10.5194/acp-20-11423-2020, 2020a.

860 Li, W. J., Shao, L. Y., Wang, W. H., Li, H., Wang, X. M., Li, Y. W., Li, W. J., Jones, T., and Zhang, D. Z.:

861   Air quality improvement in response to intensified control strategies in Beijing during 2013–2019, Sci.

862   Total Environ., 744, 140776, https://doi.org/10.1016/j.scitotenv.2020.140776, 2020b.

863 Li, Y., Miao, Y. C., Che, H. Z., and Liu, S. H.: On the heavy aerosol pollution and its meteorological

864   dependence in Shandong province, China, Atmos. Res., 256, 105572,

865   https://doi.org/10.1016/j.atmosres.2021.105572, 2021a.

866 Li, Y., Xu, H. X., Tang, K. Y., Lau, A. K. H., Fung, J. C. H., and Zhang, X. G.: An ensemble assessment of

867   the effectiveness of vehicular emission control programs for air quality improvement in Hong Kong,

868   Atmos. Environ., 262, 118571, https://doi.org/10.1016/j.atmosenv.2021.118571, 2021b.

869 Liang, X., Li, S., Zhang, S. Y., Huang, H., and Chen, S. X.: $PM_{2.5}$ data reliability, consistency, and air

870   quality assessment in five Chinese cities, J. Geophys. Res. -Atmos., 121, 10220-10236,

871   10.1002/2016JD024877, 2016.

872 Liu, B. S., Song, N., Dai, Q. L., Mei, R. B., Sui, B. H., Bi, X. H., and Feng, Y. C.: Chemical composition

873   and source apportionment of ambient $PM_{2.5}$ during the non-heating period in Taian, China, Atmos.

874   Res., 170, 23-33, https://doi.org/10.1016/j.atmosres.2015.11.002, 2016.

875 Liu, B. S., Cheng, Y., Zhou, M., Liang, D. N., Dai, Q. L., Wang, L., Jin, W., Zhang, L. Z., Ren, Y. B., Zhou,

876   J. B., Dai, C. L., Xu, J., Wang, J., Feng, Y. C., and Zhang, Y. F.: Effectiveness evaluation of temporary

877   emission control action in 2016 in winter in Shijiazhuang, China, Atmos. Chem. Phys., 18, 7019-7039,

878   https://doi.org/10.5194/acp-18-7019-2018, 2018a.

879 Liu, B. S., Wu, J. H., Wang, J., Shi, L.Y., Meng, H., Dai, Q. L., Wang, J., Song, C. B., Zhang, Y. F., Feng, Y.

880   C., and Hopke, P. K.: Chemical characteristics and sources of ambient $PM_{2.5}$ in a harbor area:

881   Quantification of health risks to workers from source-specific selected toxic elements, Environ. Pollut.,

882   268, 115926, https://doi.org/10.1016/j.envpol.2020.115926, 2021a.

883 Liu, C., Xu, R., Zhang, T. H., Zhang, H. D., Zhang, B. H., Cong, C. H., and Wu, J. Y.: Analysis of Ozone

Pollution Characteristics and Its Sources During the Shanghai Cooperation Organization Summit in Qingdao, Meteor. Environ. Sci. (in Chinese), 43, 51-58, https://doi.org/10.16765/j.cnki.1673-7148.2020.03.007, 2020a.

Liu, C., Zhang, H. D., Zhang, T. H., Xu, R., Zhang, B. H., Lu, M. Y., and Li, G. H.: The causes of ozone concentration growth in the night during the "Shanghai Cooperation Organization Summit" in Qingdao, China Environ. Sci. (in Chinese), 40, 3332-3341, https://doi.org/10.19674/j.cnki.issn1000-6923.2020.0372, 2020b.

Liu, M., Saari, R. K., Zhou, G. X., Li, J., Han, L., and Liu, X.N.: Recent trends in premature mortality and health disparities attributable to ambient $PM_{2.5}$ exposure in China: 2005–2017, Environ. Pollut., 279, 116882, https://doi.org/10.1016/j.envpol.2021.116882, 2021b.

Liu, W. J., Xu, Y. S., Liu, W. X., Liu, Q. Y., Yu, S. Y., Liu, Y., Wang, X., and Tao, S.: Oxidative potential of ambient $PM_{2.5}$ in the coastal cities of the Bohai Sea, northern China: Seasonal variation and source apportionment, Environ. Pollut., 236, 514-528, https://doi.org/10.1016/j.envpol.2018.01.116, 2018b.

Liu, F., Beirle, S., Zhang, Q., van der, A. R. J., Zheng, B., Tong, D., and He, K.: NOx emission trends over Chinese cities estimated from OMI observations during 2005 to 2015, Atmos. Chem. Phys., 17, 9261-9275, https://doi.org/10.5194/acp-17-9261-2017, 2017.

Lyu, X. P., Zeng, L.W., Guo, H., Simpson, I. J., Ling, Z. H., Wang, Y., Murray, F., Louie, P. K. K., Saunders, S. M., Lam, S. H. M., and Blake, D. R.: Evaluation of the effectiveness of air pollution control measures in Hong Kong, Environ. Pollut., 220, 87-94, https://doi.org/10.1016/j.envpol.2016.09.025, 2017.

Ma, X. W., Li, C. D., Dong, X. Y., and Liao, H.: Empirical analysis on the effectiveness of air quality control measures during mega events: Evidence from Beijing, China, J. Clean Prod., 271, 122536, https://doi.org/10.1016/j.jclepro.2020.122536, 2020.

Ma, X. D., Huang, J. P., Zhao, T. L., Liu, C., Zhao, K. H., Xing, J., and Xiao, W.: Rapid increase in summer surface ozone over the North China plain during 2013–2019: a side effect of particulate matter reduction control? Atmos. Chem. Phys., 21, 1-16, https://doi.org/10.5194/acp-21-1-2021, 2021.

Manousakas, M., Papaefthymiou, H., Diapouli, E., Migliori, A., Karydas, A. G., Bogdanovic-Radovic, I., and Eleftheriadis, K.: Assessment of $PM_{2.5}$ sources and their corresponding level of uncertainty in a coastal urban area using EPA PMF 5.0 enhanced diagnostics, Sci. Total Environ., 574, 155-164, https://doi.org/10.1016/j.scitotenv.2016.09.047, 2017.

Masiol, M., Squizzato, S., Rich, D. Q., and Hopke, P. K.: Long-term trends (2005–2016) of source apportioned $PM_{2.5}$ across New York State, Atmos. Environ., 201, 110-120, https://doi.org/10.1016/j.atmosenv.2018.12.038, 2019.

Meng, Z. Y., Ding, G. A., Xu, X. B., Xu, X. D., Yu, H. Q., and Wang, S. F.: Vertical distributions of SO_2 and NO_2 in the lower atmosphere in Beijing urban areas, China, Sci. Total Environ., 390, 456-465, https://doi.org/10.1016/j.scitotenv.2007.10.012, 2008.

Munir, S., Chen, H. B., and Ropkins, K.: Quantifying temporal trends in ground level ozone concentration in the UK, Sci. Total Environ., 458-460, 217-227, https://doi.org/10.1016/j.scitotenv.2013.04.045, 2013.

Nøjgaard, J. K., Nguyen, Q. T., Glasius, M., and Sørensen, L. L.: Nucleation and Aitken mode atmospheric particles in relation to O_3 and NO_X at semirural background in Denmark, Atmos. Environ., 49, 275-283, https://doi.org/10.1016/j.atmosenv.2011.11.040, 2012.

Nirel, R., and Dayan, U.: On the Ratio of Sulfur Dioxide to Nitrogen Oxides as an Indicator of Air Pollution Sources, J. Appl. Meteorol., 40, 1209-1222, https://doi.org/10.1175/1520-

928   0450(2001)040<1209:OTROSD>2.0.CO;2, 2001.

Paatero, P., and Tapper, U.: Positive matrix factorization: A non-negative factor model with optimal
    utilization of error estimates of data values. Environmetrics, 5, 111-126,
    https://doi.org/10.1002/env.3170050203, 1994.

Police, S., Sahu, S. K., and Pandit, G. G.: Chemical characterization of atmospheric particulate matter and
    their source apportionment at an emerging industrial coastal city, Visakhapatnam, India, Atmos. Pollut.
    Res., 7, 725-733, https://doi.org/10.1016/j.apr.2016.03.007, 2016.

Pugliese, S. C., Murphy, J. G., Geddes, J. A., and Wang, J. M.: The impacts of precursor reduction and
    meteorology on ground-level ozone in the Greater Toronto Area, Atmos. Chem. Phys., 14, 8197-8207,
    https://doi.org/10.5194/acp-14-8197-2014, 2014.

Qi, L., Zhang, Y. F., Ma, Y. H., Chen, M. D., Ge, X. L., Ma, Y., Zheng, J., Wang, Z., and Li, S. Z.: Source
    identification of trace elements in the atmosphere during the second Asian Youth Games in Nanjing,
    China: Influence of control measures on air quality, Atmos. Pollut. Res., 7, 547-556,
    https://doi.org/10.1016/j.apr.2016.01.003, 2016.

Querol, X., Viana, M., Alastuey, A., Amato, F., Moreno, T., Castillo, S., Pey, J., de la Rosa, J., Sánchez de
    la Campa, A., Artíñano, B., Salvador, P., García Dos Santos, S., Fernández-Patier, R., Moreno-Grau,
    S., Negral, L., Minguillón, M. C., Monfort, E., Gil, J. I., Inza, A., Ortega, L. A., Santamaría, J. M., and
    Zabalza, J.: Source origin of trace elements in PM from regional background, urban and industrial
    sites of Spain, Atmos. Environ., 41, 7219-7231, https://doi.org/10.1016/j.atmosenv.2007.05.022, 2007.

Ryou, H. G., Heo, J., and Kim, S. Y.: Source apportionment of PM_{10} and $PM_{2.5}$ air pollution, and possible
    impacts of study characteristics in South Korea, Environ. Pollut., 240, 963-972,
    https://doi.org/10.1016/j.envpol.2018.03.066, 2018.

Sen, P. K.: Estimates of the Regression Coefficient Based on Kendall's Tau AU – Sen, Pranab Kumar, J.
    Am. Stat. Assoc., 63, 1379-1389, https://doi.org/10.1080/01621459.1968.10480934, 1968.

Schleicher, N., Norra, S., Chen, Y., Chai, F., and Wang, S.: Efficiency of mitigation measures to reduce
    particulate air pollution—A case study during the Olympic Summer Games 2008 in Beijing, China,
    Sci. Total Environ., 427-428, 146-158, https://doi.org/10.1016/j.scitotenv.2012.04.004, 2012.

Shi, Z. B., Song, C. B., Liu, B. W., Lu, G. D., Xu, J. S., Vu, T. V., Elliott, R. J. R., Li, W. J., Bloss, W. J.,
    and Harrison, R. M.: Abrupt but smaller than expected changes in surface air quality attributable to
    COVID-19 lockdowns, Sci Adv., 7, eabd6696, https://doi.org/10.1126/sciadv.abd6696, 2021.

Sofowote, U. M., Healy, R. M., Su, Y., Debosz, J., Noble, M., Munoz, A., Jeong, C. H., Wang, J. M., Hilker,
    N., Evans, G. J., Brook, J. R., Lu, G., and Hopke, P. K.: Sources, variability and parameterizations of
    intra-city factors obtained from dispersion-normalized multi-time resolution factor analyses of $PM_{2.5}$
    in an urban environment, Sci. Total Environ., 761, 143225,
    https://doi.org/10.1016/j.scitotenv.2020.143225, 2021.

Song, L. L., Dai, Q. L., Feng, Y. C., and Hopke, P. K.: Estimating uncertainties of source contributions to
    $PM_{2.5}$ using moving window evolving dispersion normalized PMF, Environ. Pollut., 286, 117576,
    https://doi.org/10.1016/j.envpol.2021.117576, 2021.

Sujatha, P., Mahalakshmi, D. V., Ramiz, A., Rao, P. V. N., and Naidu, C.V.: Ventilation coefficient and
    boundary layer height impact on urban air quality, Cogent Environ. Sci., 2, 1125284
    https://doi.org/10.1080/23311843.2015.1125284, 2016.

Tao, J., Gao, J., Zhang, L., Zhang, R., Che, H., Zhang, Z., Lin, Z., Jing, J., Cao, J., and Hsu, S. C.: $PM_{2.5}$
    pollution in a megacity of southwest China: source apportionment and implication, Atmos. Chem.
    Phys., 14, 8679-8699, https://doi.org/10.5194/acp-14-8679-2014, 2014.

Tian, Y. Z., Wang, J., Peng, X., Shi, G. L., and Feng, Y.C.: Estimation of the direct and indirect impacts of fireworks on the physicochemical characteristics of atmospheric PM_{10} and $PM_{2.5}$, Atmos. Chem. Phys., 14, 9469-9479, https://doi.org/10.5194/acp-14-9469-2014, 2014.

Tsai, P. J., Young, L. H., Hwang, B. F., Lin, M. Y., Chen, Y. C., and Hsu, H.T.: Source and health risk apportionment for $PM_{2.5}$ collected in Sha-Lu area, Taiwan, Atmos. Pollut. Res., 11, 851-858, https://doi.org/10.1016/j.apr.2020.01.013, 2020.

Tsai, D. H., Wang, J. L., Chuang, K. J., and Chan, C. C.: Traffic-related air pollution and cardiovascular mortality in central Taiwan, Sci. Total Environ., 408, 1818-1823, https://doi.org/10.1016/j.scitotenv.2010.01.044, 2010.

Vodonos, A., and Schwartz, J.: Estimation of excess mortality due to long-term exposure to $PM_{2.5}$ in continental United States using a high-spatiotemporal resolution model, Environ. Res., 196, 110904, https://doi.org/10.1016/j.envres.2021.110904, 2021.

Vu, T. V., Shi, Z. B., Cheng, J., Zhang, Q., He, K. B., Wang, S. X., and Harrison, R. M.: Assessing the impact of clean air action on air quality trends in Beijing using a machine learning technique, Atmos. Chem. Phys., 19, 11303-11314, https://doi.org/10.5194/acp-19-11303-2019, 2019.

Wang, D. F., Zhou, B., Fu, Q. Y., Zhao, Q. B., Zhang, Q., Chen, J. M., Yang, X., Duan, Y. S., and Li, J.: Intense secondary aerosol formation due to strong atmospheric photochemical reactions in summer: observations at a rural site in eastern Yangtze River Delta of China, Sci. Total Environ., 571, 1454-1466, https://doi.org/10.1016/j.scitotenv.2016.06.212, 2016.

Wang, H. L., Miao, Q., Shen, L. J., Yang, Q., Wu, Y. Z., and Wei, H.: Air pollutant variations in Suzhou during the 2019 novel coronavirus (COVID-19) lockdown of 2020: High time-resolution measurements of aerosol chemical compositions and source apportionment, Environ. Pollut., 271, 116298, https://doi.org/10.1016/j.envpol.2020.116298, 2021a.

Wang, S. X., Xing, J., Zhao, B., Jang, C., and Hao, J. M.: Effectiveness of national air pollution control policies on the air quality in metropolitan areas of China, J. Environ. Sci., 26, 13-22, https://doi.org/10.1016/S1001-0742(13)60381-2, 2014.

Wang, Y., Xue, Y. F., Tian, H. Z., Gao, J., Chen, Y., Zhu, C. Y., Liu, H. J., Wang, K., Hua, S. B., Liu, S. H., and Shao, P. Y.: Effectiveness of temporary control measures for lowering $PM_{2.5}$ pollution in Beijing and the implications, Atmos. Environ., 157, 75-83, https://doi.org/10.1016/j.atmosenv.2017.03.017, 2017.

Wang, Y. Q., Zhang, X. Y., and Draxler, R.: TrajStat: GIS-based software that uses various trajectory statistical analysis methods to identify potential sources from long-term air pollution measurement data, Environ. Model. Softw., 24, 938-939, https://doi.org/10.1016/j.envsoft.2009.01.004, 2009.

Wang, Y. Y., Liu, B. S., Zhang, Y. F., Dai, Q. L., Song, C. B., Duan, L. Q., Guo, L. L., Zhao, J., Xue, Z. G., Bi, X. H., and Feng, Y. C.: Potential health risks of inhaled toxic elements and risk sources during different COVID-19 lockdown stages in Linfen, China, Environ. Pollut., 284, 117454, https://doi.org/10.1016/j.envpol.2021.117454, 2021b.

Xu, H., Xiao, Z. M., Chen, K., Tang, M., Zheng, N. Y., Li, P., Yang, N., Yang, W., and Deng, X. W.: Spatial and temporal distribution, chemical characteristics, and sources of ambient particulate matter in the Beijing-Tianjin-Hebei region, Sci. Total Environ., 658, 280-293, https://doi.org/10.1016/j.scitotenv.2018.12.164, 2019a.

Xu, L. L., Jiao, L., Hong, Z. Y., Zhang, Y. R., Du, W. J., Wu, X., Chen, Y. T., Deng, J. J., Hong, Y. W., and Chen, J. S.: Source identification of $PM_{2.5}$ at a port and an adjacent urban site in a coastal city of China: Impact of ship emissions and port activities, Sci. Total Environ., 634, 1205-1213,

1016   https://doi.org/10.1016/j.scitotenv.2018.04.087, 2018.

1017 Xu, M., Qin, Z. F., Zhang, S. H., and Xie, Y.: Health and economic benefits of clean air policies in China:
1018   A case study for Beijing-Tianjin-Hebei region, Environ. Pollut., 285, 117525,
1019   https://doi.org/10.1016/j.envpol.2021.117525, 2021.

1020 Xu, W., Liu, X. J., Liu, L., Dore, A. J., Tang, A., Lu, L., Wu, Q. H., Zhang, Y. Y., Hao, T. X., Pan, Y.
1021   P., Chen, J. M., and Zhang, F. S.: Impact of emission controls on air quality in Beijing during APEC
1022   2014: Implications from water-soluble ions and carbonaceous aerosol in $PM_{2.5}$ and their precursors,
1023   Atmos. Environ., 210, 241-252, https://doi.org/10.1016/j.atmosenv.2019.04.050, 2019b.

1024 Yin, H., Liu, C., Hu, Q. H., Liu, T., Wang, S., Gao, M., Xu, S. Q., Zhang, C. X., and Su, W. J.: Opposite
1025   impact of emission reduction during the COVID-19 lockdown period on the surface concentrations of
1026 $PM_{2.5}$ and O_3 in Wuhan, China, Environ. Pollut., 289, 117899,
1027   https://doi.org/10.1016/j.envpol.2021.117899, 2021.

1028 Yang, S., Duan, F., Ma, Y., Li, H., Ma, T., Zhu, L., Huang, T., Kimoto, T., and He, K.: Mixed and intensive
1029   haze pollution during the transition period between autumn and winter in Beijing, China, Sci. Total
1030   Environ., 711, 134745, https://doi.org/10.1016/j.scitotenv.2019.134745, 2020.

1031 Yu, M. F., Zhu, Y., Lin, C. J., Wang, S. X., Xing, J., Jang, C., Huang, J. Z., Huang, J. Y., Jin, J. B., and Yu,
1032   L.: Effects of air pollution control measures on air quality improvement in Guangzhou, China, J.
1033   Environ. Manage., 244, 127-137, https://doi.org/10.1016/j.jenvman.2019.05.046, 2019.

1034 Zhai, S., Jacob, D. J., Wang, X., Shen, L., Li, K., and Zhang, Y.: Fine particulate matter ($PM_{2.5}$) trends in
1035   China, 2013–2018: separating contributions from anthropogenic emissions and meteorology, Atmos.
1036   Chem. Phys., 19, 11031-11041, https://doi.org/10.5194/acp-19-11031-2019, 2019.

1037 Zhang, D. Z., Shi, G. Y., Iwasaka, Y., Hu, M., and Zang, J. Y.: Anthropogenic Calcium Particles Observed
1038   in Beijing and Qingdao, China, Water, Air, & Soil Pollution: Focus., 5, 261-276,
1039   https://doi.org/10.1007/s11267-005-0743-y, 2005.

1040 Zhang, Q., He, K. B., and Huo, H.: Cleaning China's air. Nature, 484, 161-162,
1041   https://doi.org/10.1038/484161a, 2012.

1042 Zhang, Q., Zheng, Y. X., Tong, D., Shao, M., Wang, S. X., Zhang, Y. H., Xu, X. D., Wang, J. N., He,
1043   H., Liu, W. Q., Ding, Y. H., Lei, Y., Li, J. H., Wang, Z. F., Zhang, X. Y., Wang, Y. S., Cheng, J., Liu,
1044   Y., Shi, Q. R., Yan, L., Geng, G. N., Hong, C. P., Li, M., Liu, F., Zheng, B., Cao, J. J., Ding, A. J., Gao,
1045   J., Fu, Q. Y., Huo, J. T., Liu, B. X., Liu, Z. R., Yang, F. M., He, K. B., and Hao, J.M.: Drivers of
1046   improved $PM_{2.5}$ air quality in China from 2013 to 2017, Proceedings of the National Academy of
1047   Sciences, 116, 24463-24469, https://doi.org/10.1073/pnas.1907956116, 2019.

1048 Zhang, Y., Yang, L. X., Bie, S. J., Zhao, T., Huang, Q., Li, J. S., Wang, P. C., Wang, Y. M., and Wang, W.
1049   X.: Chemical compositions and the impact of sea salt in atmospheric PM_1 and $PM_{2.5}$ in the coastal
1050   area, Atmos. Res., 250, 105323, https://doi.org/10.1016/j.atmosres.2020.105323, 2021.

1051 Zhao, C. K., Sun, Y., Zhong, Y. P., Xu, S. H., Liang, Y., Liu, S., He, X. D., Zhu, J. H., Shibamoto, T., and
1052   He, M.: Spatio-temporal analysis of urban air pollutants throughout China during 2014–2019, Air
1053   Qual. Atmos. Hlth., 14, 1619-1632, https://doi.org/10.1007/s11869-021-01043-5, 2021a.

1054 Zhao, S., Tian, H. Z., Luo, L. N., Liu, H. J., Wu, B. B., Liu, S. H., Bai, X. X., Liu, W., Liu, X. Y., Wu, Y.
1055   M., Lin, S. M., Guo, Z. H., Lv, Y. Q., and Xue, Y. F.: Temporal variation characteristics and source
1056   apportionment of metal elements in $PM_{2.5}$ in urban Beijing during 2018–2019, Environ. Pollut., 268,
1057   115856, https://doi.org/10.1016/j.envpol.2020.115856, 2021b.

1058 Zong, Z., Wang, X. P., Tian, C. G., Chen, Y. J., Fu, S. F., Qu, L., Ji, L., Li, J., and Zhang, G.: PMF and
1059   PSCF based source apportionment of $PM_{2.5}$ at a regional background site in North China, Atmos. Res.,

1060   203, 207-215, https://doi.org/10.1016/j.atmosres.2017.12.013, 2018.

1061

1062

1063

1064
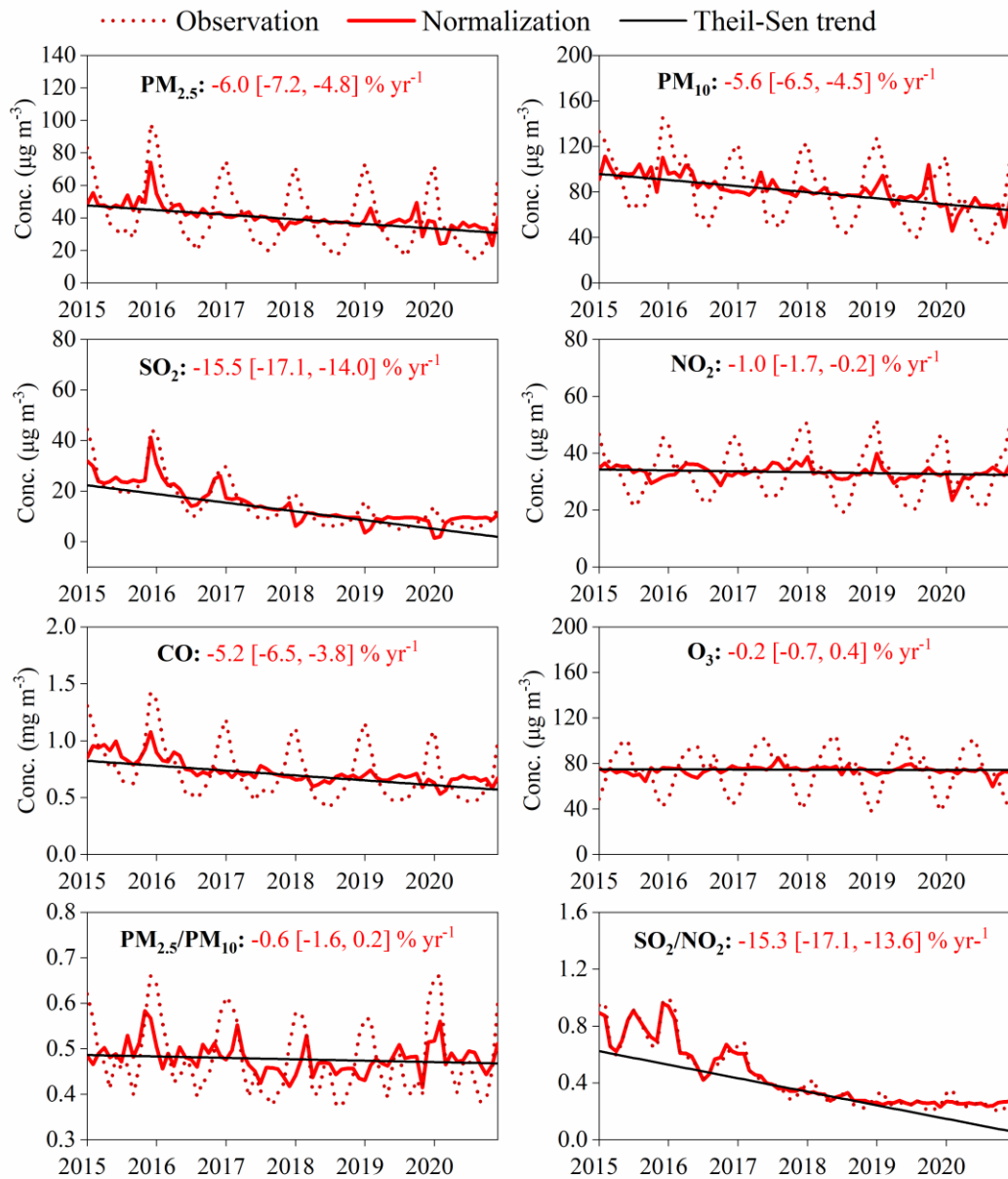
Figure 1. Trends of air pollutant concentrations and $PM_{2.5}/PM_{10}$ and SO_2/NO_2 from 2015 to 2020. "Observation" represents the observed data, and "Normalization" in represents the modelled concentrations of air pollutants after weather normalization. The black line shows the Theil–Sen trend after weather normalization.

1069

1070

1071
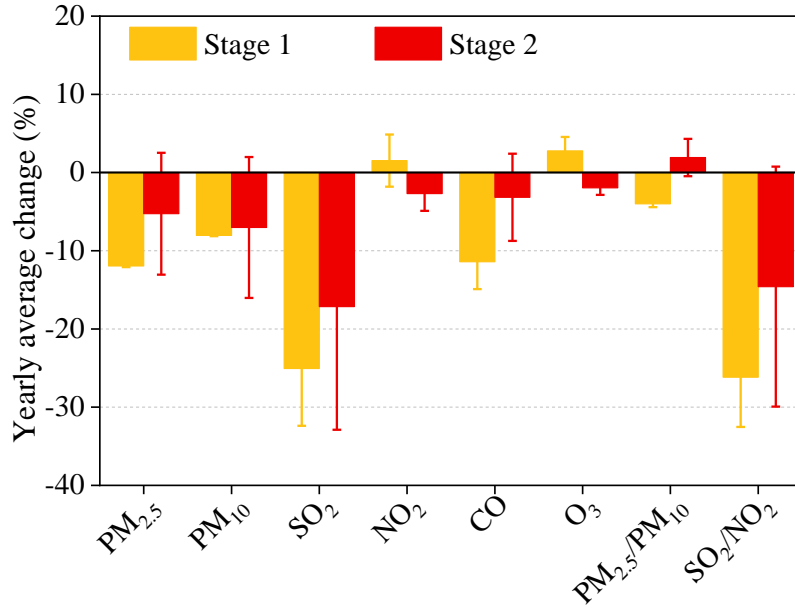
Figure 2. Yearly average change of air pollutants and PM₂.₅/PM₁₀ and SO₂/NO₂ during
different pollution-control stages based on the weather normalized data.

1074

1075
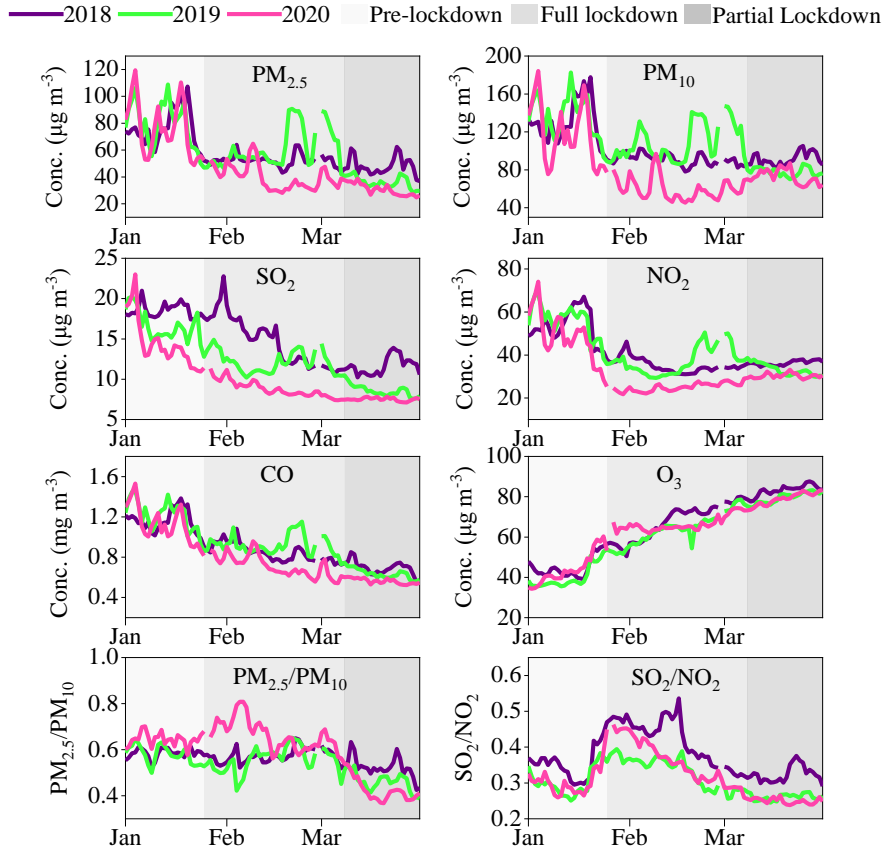
Figure 3. Time series of air pollutants concentrations and PM₂.₅/PM₁₀ and SO₂/NO₂ during
the different stages of COVID-19 lockdown start dates or equivalent in 2020 versus 2018 and
2019 based on the weather normalization data.

1079

1080

1081
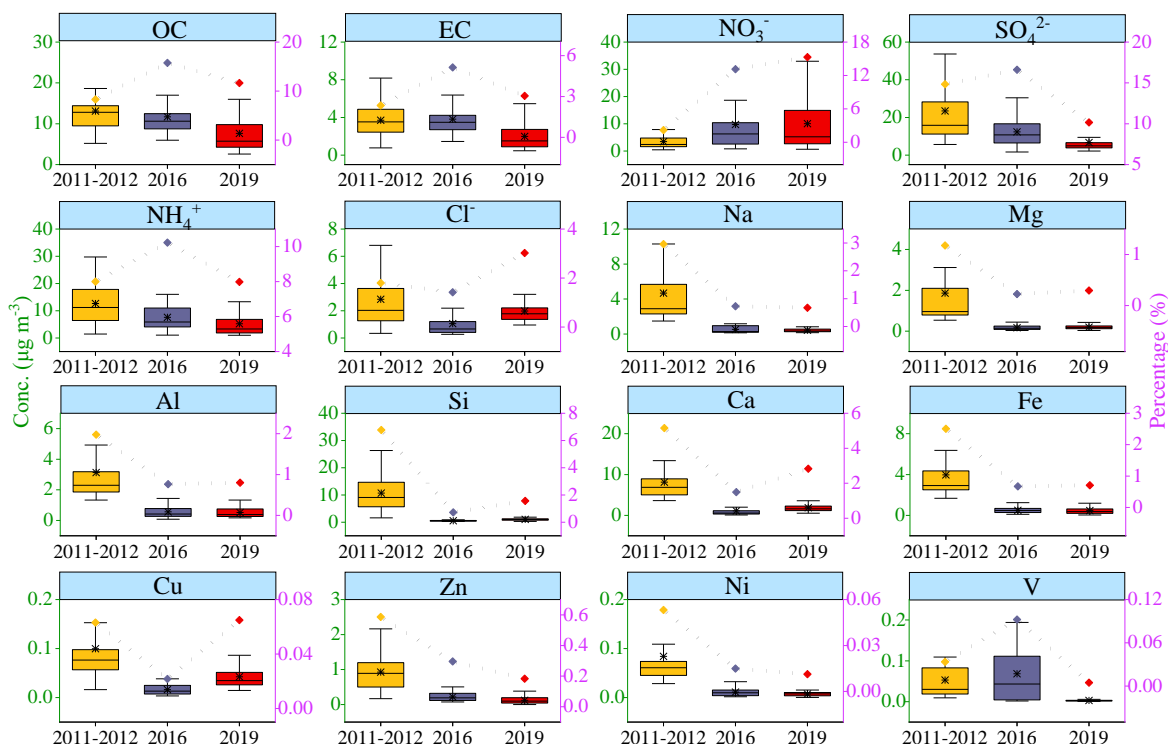
Figure 4. Variations of the average concentrations and percentages of major chemical compositions of PM$_{2.5}$ in 2011-2012, 2016, and 2019. Box charts represent concentrations, and line charts represent percentages.

1085

1086
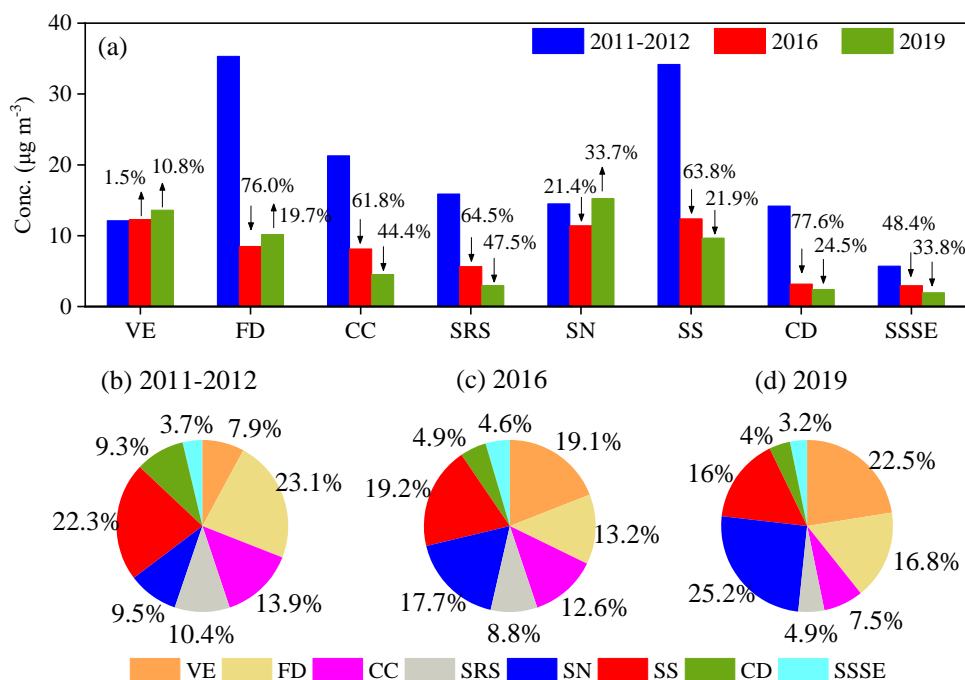
Figure 5. Changes in source contributions for 2011-2012, 2016, and 2019. VE represents vehicle emissions, FD represents fugitive dust, CC represents coal combustion, SRS represents steel-related smelting, SN represents secondary nitrate, SS represents secondary sulphate, CD represents construction dust, and SSSE represents sea salt and ship emissions.
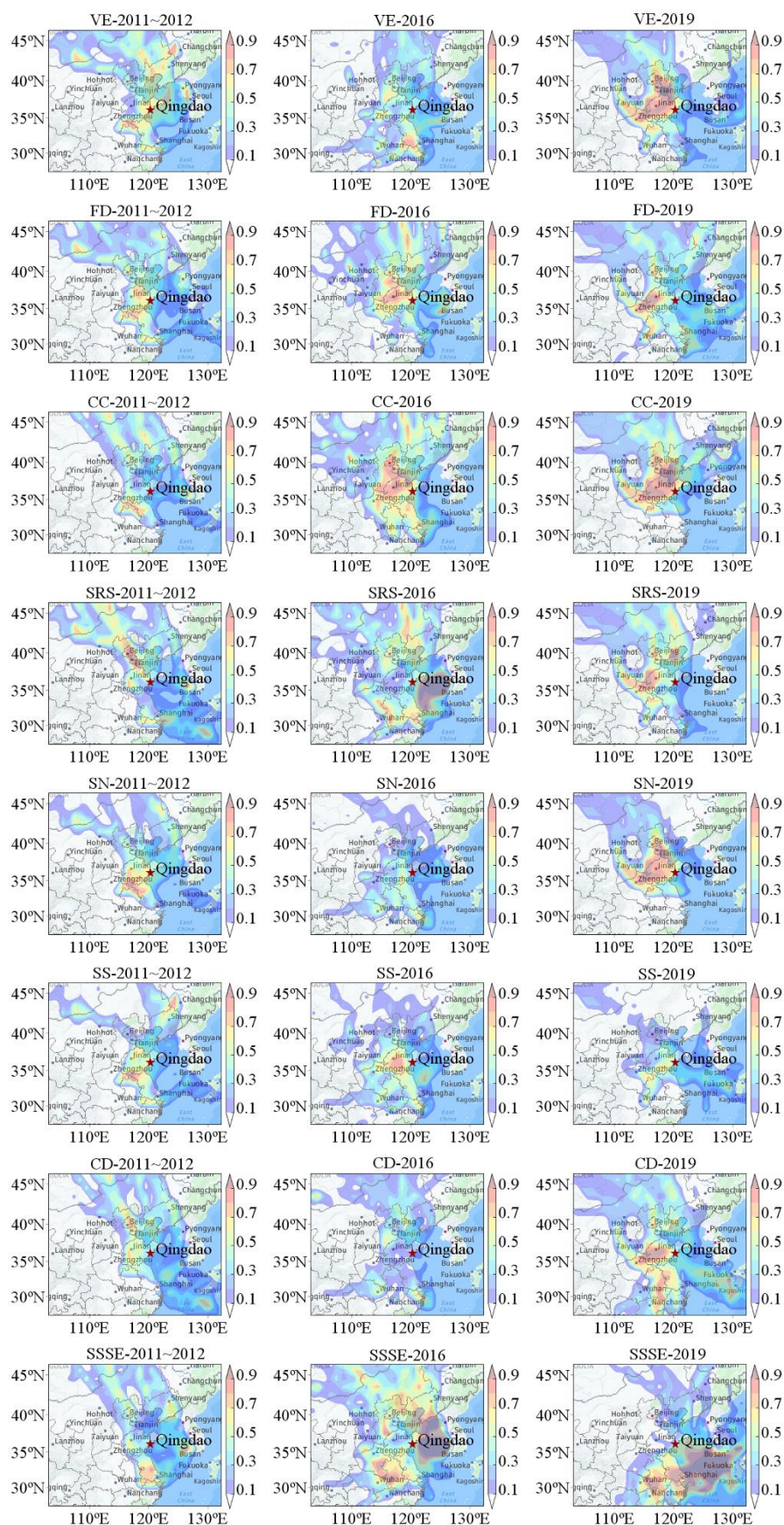
Figure 6. WPSCF plots for various emission sources during different periods (base map from Yahoo Maps). VE represents vehicle emissions, FD represents fugitive dust, CC represents

1094   coal combustion, SRS represents steel-related smelting, SN represents secondary nitrate, SS

1095   represents secondary sulphate, CD represents construction dust, and SSSE represents sea salt

1096   and ship emissions.

1097